HHS Public Access

Author manuscript

J Immunol. Author manuscript; available in PMC 2022 August 15.

Published in final edited form as:

J Immunol. 2021 August 15; 207(4): 1165–1179. doi:10.4049/jimmunol.2001286.

Postnatal ozone exposure disrupts alveolar development, exaggerates mucoinflammatory responses, and suppresses bacterial clearance in developing *Scnn1b*-Tg+ mice lungs

Ishita Choudhary[*], **Thao Vo**[*], **Kshitiz Paudel**[*], **Radha Yadav**[*], **Yun Mao**[*], **Sonika Patial**[*], **Yogesh Saini**[*,¶]

[*]Department of Comparative Biomedical Sciences, School of Veterinary Medicine, Louisiana State University, Baton Rouge, LA 70803, USA.

Abstract

Increased levels of ambient ozone, one of the six criteria air pollutants, result in respiratory tract injury and worsening of ongoing lung diseases. However, the effect of ozone exposure on the respiratory tract undergoing active lung development and simultaneously experiencing mucoinflammatory lung diseases such as cystic fibrosis (CF) remains unclear. To address these questions, we exposed *Scnn1b* transgenic (*Scnn1b*-Tg+), a mouse model of CF-like lung disease, and littermate WT mice to ozone from postnatal day (PND) 3-20 and examined the lung phenotypes at PND21. As compared to filtered air (FA)-exposed WT mice, the ozone-exposed WT mice exhibited marked alveolar space enlargement, in addition to significant eosinophilic infiltration, Type 2 inflammation, and mucous cell metaplasia. Ozone-exposed *Scnn1b*-Tg+ mice also exhibited significantly increased alveolar space enlargement which was also accompanied by exaggerated granulocytic infiltration, type 2 inflammation, and a greater degree of mucoobstruction. The alveolar space enlargement in ozone-exposed WT, FA-exposed *Scnn1b*-Tg+, and ozone-exposed *Scnn1b*-Tg+ mice was accompanied by elevated levels of MMP12 protein in macrophages and *Mmp12* mRNA in the lung homogenates. Finally, while bacterial burden was largely resolved by PND21 in FA-exposed *Scnn1b*-Tg+ mice, ozone-exposed *Scnn1b*-Tg+ mice exhibited compromised bacterial clearance which was also associated with increased levels of IL-10, an immunosuppressive cytokine, and marked mucoobstruction. Taken together, our data show that ozone exposure results in alveolar space remodeling during active phases of lung development and markedly exaggerates the mucoinflammatory outcomes of pediatric-onset lung disease including bacterial infections, granulocytic inflammation, mucus obstruction, and alveolar space enlargement.

[¶]**Corresponding author:** *Yogesh Saini, DVM, MVSc, PhD*, Department of Comparative Biomedical Sciences, School of Veterinary Medicine, Louisiana State University, Baton Rouge, LA 70803, USA, Phone: 225-578-9143, Fax: 225-578-9895, ysaini@lsu.edu.

Author Contributions

Y. S. and S. P. conceived and designed the research; I.C., T. V., and Y. S. maintained the animal colony, conducted animal necropsies, and performed BALF cellularity assays; I. C., T. V, K. P., R. Y., Y. M., S. P., and Y. S. performed cytokine, gene expression assays, microbiological, and histopathological experiments; S. P. performed histopathological analyses; I. C., S. P., and Y. S. wrote and reviewed the manuscript for intellectual contents.

Disclosures: The authors have no conflicts of interest to disclose.

Keywords

Ozone; Lung; Mucus obstruction; Mucous cell metaplasia; Bacterial clearance

Introduction

Ozone, a highly reactive oxidant gas, is one of the common environmental air pollutants (1). Ozone reduces lung function (2, 3), increases risks for asthma (4-6), and exacerbates pulmonary symptoms in mucoinflammatory diseases including cystic fibrosis (CF) (7, 8), chronic obstructive pulmonary disease (9), and asthma (10). Increased ambient ozone levels pose serious health hazards, especially for young children who spend a considerable amount of time playing outdoors (11). It has been reported that young children, with their lung development still underway, are more vulnerable to environmental toxicants because of their higher respiratory rates that allow them to rapidly inhale toxicants (12, 13). However, the superimposed effect of ozone on the progression of impending mucoinflammatory lung disease in developing lungs has never been tested, thus the requirement for further experimentation.

CF is a chronic, progressive respiratory disease that primarily affects the respiratory system in children and young adults. Although a number of mouse models with CFTR mutation have been developed, none of them recapitulate features of human CF-like lung disease (14). This is likely due to the dominance of calcium-activated chloride channels (CaCCs) in murine airways (15) that compensate for the alterations caused by CFTR dysfunction or deletion. The *Scnn1b*-Tg+ mouse, a well-accepted model for human CF-like lung disease, overexpresses a transgene encoding sodium channel, non-voltage gated 1, beta subunit (*Scnn1b*) in the club cells (16). As a result of airway epithelial-specific overexpression of *Scnn1b* transgene and its protein product, i.e., beta subunit, epithelial sodium ion (Na^+) channel (βENaC), the absorption of Na^+ is increased in the epithelial cells. Due to increased ionic concentration of Na^+ in the epithelial cells, the buildup of osmotic gradient drives the movement of water from airway surface liquid layer (ASL) into the epithelial cells, which leads to ASL layer dehydration (16, 17). As a result, within the first week of postnatal life, the *Scnn1b*-Tg+ mice develop human CF-like lung disease with features such as mucostasis, mucus obstruction, airway inflammation, mucous cell metaplasia, (MCM), and poor mucociliary clearance (17). As a result of poor mucociliary clearance, the *Scnn1b*-Tg+ mice also manifest spontaneous bacterial infections and impaired bacterial clearance (18, 19). The airway inflammation in *Scnn1b*-Tg+ mice is characterized by the presence of increased numbers of activated macrophages, neutrophils, eosinophils, and lymphocytes in the airspaces (16, 17, 19). Taken together, the early initiation of the mucoinflammatory pathology and its close resemblance to human-CF-like disease, the *Scnn1b*-Tg+ mouse can be utilized to study the initiation and progression of pediatric lung diseases.

Several studies done in the past have investigated the effects of environmental toxicants including nanoparticles, fungal spores, mainstream tobacco smoke, and secondhand smoke in *Scnn1b*-Tg+ mice (20-24). Three epidemiological studies report that exposure to ozone increases the risk of pulmonary exacerbations in CF patients (7, 8, 25) but, to the best of

our knowledge, no studies have been conducted to examine the effects of ozone exposure on the initiation and progression of airway disease in *Scnn1b*-Tg+ mice. Thus, the effect of ozone on key characteristics of *Scnn1b*-Tg+ mice, i.e., airspace inflammation, spontaneous bacterial infection, mucus hypersecretion, and MCM remain unexplored and warrants investigation especially in neonates where the lung is in the developing stages.

To study the interactions between ozone exposure and mucoinflammatory disease in *Scnn1b*-Tg+ mice, we hypothesized that ozone exposure from postnatal day (PND) 3-20 will perturb normal lung homeostasis in WT neonates and exaggerate *Scnn1b*-Tg+ lung pathology. Accordingly, we exposed *Scnn1b*-Tg+ and WT littermates to ozone from PND3-20 and examined lung phenotypes at the weaning age of PND21. Since *Scnn1b*-Tg+ mice exhibit airway inflammation (16, 17), bacterial infections (18, 19), and profound type 2 immune response (17), we measured these attributes by assessing BALF cellularity, cytokine levels, bacterial CFU counts in BALF, mucus obstruction, MCM, mucins expression, and gene expression relevant to Type 2 mucoinflammatory responses. The results from these studies provide novel insights into the effects of early postnatal ozone exposure on lung development and the manifestation of responses associated with muco-obstructive lung diseases.

Materials and Methods

Scnn1b-Tg+ mice and animal husbandry

Scnn1b-Tg+ mice [*Tg (Scgb1a1-Scnn1b)6608Bouc/J*] were procured from Jackson Laboratory (Bar Harbor, ME) on congenic C57BL/6J background and were maintained on this background by selective breeding between WT (*Scnn1b*-Tg−) and *Scnn1b*-Tg+ mice. All the mice used in this study were genotyped for *Scnn1b* transgene using polymerase chain reaction (PCR) as reported previously (24). Mice were maintained in hot washed, individually ventilated cages on a 12h dark/light cycle at the Division of Laboratory Animal Medicine (DLAM) at Louisiana State University, Baton Rouge, LA. Mice were supplied with food and water ad libitum except during filtered air (FA) or ozone exposure (4 h/day). All animal use and inhalation procedures were approved by the Institutional Animal Care and Use Committee (IACUC) of the Louisiana State University.

Ozone and filter air exposure

Three-day-old neonates (entire litter) were transferred to individual cages with perforated lids and were exposed to either FA or 800 ppb ozone (798 ± 8.561 (SEM) ppb) for 4 hours. Following 4 hours of exposure each evening to either FA or ozone, mice were returned to their parental cages. Ozone concentration was monitored during the entire experimental period (PND3-20) of 4 hours/day exposure. Mice were exposed in the nightly conditions (high physical activity) (26, 27), which simulates real-life scenarios of the higher activity phase in humans, as detailed previously (28). Loading of animals into the light-protected chambers was coordinated with the start of the night cycle at the vivarium. The timing of exposures was maintained strictly and consistently for all the exposures that lasted for 18 consecutive days.

Tissue harvesting and Bronchoalveolar lavage fluid (BALF) analyses

FA- or ozone-exposed mice (PND 21) were anesthetized via intraperitoneal (IP) injection of 2,2,2-tribromoethanol (Millipore Sigma, Burlington, MA) and BALF was harvested aseptically as described previously (18). 60 μl of BALF fluid was taken for colony forming units (CFU) enumeration and the remaining BALF was centrifuged in a cooling centrifuge at 500 g for 5 min. Cell-free BALF supernatant was collected and stored at −80°C for cytokine and immunoglobulins (Ig) analyses. Cell pellets were resuspended in 250 μl of phosphate-buffered saline (PBS). 50 μl of cell suspension was used for total cell counts using a hemocytometer (Bright-Line, Horsham, PA) and 200 μl was used to make cytospins followed by differential staining (Modified Giemsa Kit; Newcomer Supply, Middleton, WI). Cytospins were analyzed for the determination of macrophage surface area. Briefly, photographs were captured under 20X objective of the ECLIPSE Ci-L microscope with DS-Fi2 camera attachment (Nikon, Melville, NY). Thereafter, captured images were processed using the ImageJ software (NIH) to determine the surface area of the macrophages (29). Unlavaged left lung lobes were stored in 10% neutral buffered formalin and lavaged right lung lobes were stored at −80°C for gene expression and cytokine analyses.

Cytokines and Immunoglobulins analyses

Cell-free BALF was assayed for keratinocyte chemokine (KC/CXCL1), macrophage inflammatory protein 2 (MIP-2 /CXCL2), granulocyte-colony stimulating factor (G-CSF), monocyte chemokine protein-1(MCP-1/CCL2), macrophage inflammatory protein 1-alpha (MIP-1α/CCL3), macrophage inflammatory protein 1-beta (MIP-1β/CCL4), IL-4, IL-5, IL-6, IL-13, IL-17, IP-10, IL-1α, IL-1β, and IL-10 using Luminex-XMAP-based assay (MCYTOMAG-70K) according to the manufacturer's instructions (EMD Millipore, Billerica, MA). To assess the levels of eosinophilic inflammation relevant cytokines, i.e., Eotaxin, CCL7, CCL12, CCL17, CCL22, CCL24 (BioPlex Pro Mouse Chemokine panel, Hercules, CA), we used lung homogenates because of the unavailability of enough BALF sample. The data were normalized to the total protein concentration. Total protein contents in the BALF were determined by Bradford assay (Bio-Rad, Hercules, CA). Total dsDNA contents were determined spectrophotometrically, using Nanodrop 8000 (Thermo Scientific, Waltham, MA). Immunoglobulin concentrations in the cell-free BALF were determined with MILLIPLEX MAP mouse immunoglobulin isotyping magnetic bead panel isotyping multiplex assay (MGAMMAG-300K) according to the manufacturer's instructions (EMD Millipore, Billerica, MA).

BALF microbiology

To estimate the bacterial burden in the BALF, aseptically harvested cell-free BALF (60 μl) was serially diluted onto Columbia blood agar (CBA) plates (Hardy Diagnostics, Santa Maria, CA) and incubated in anaerobic candle jars at 37°C as previously described (24). CFUs were counted at 48 hours post-incubation and physical characteristics of colonies including size, shape, color, margins, and elevation, were recorded.

Histopathology

Unlavaged left lung lobes were stored in 10% neutral buffered formalin for fixation. Subsequently, formalin-fixed tissues were paraffin-embedded, sectioned at 5μm, and processed for histopathological analyses. Hematoxylin and eosin (H&E) staining was performed to access the structural and morphological alterations in the left lung. Alcian blue-periodic acid-Schiff (AB-PAS) staining was performed to examine the airway mucus contents and the mucous cells. All the slides were graded by a board-certified anatomic pathologist in a blinded manner using the histological semi-quantitative grading strategy as previously described (30, 31).

Immunohistochemistry

Immunohistochemical staining for Major Basic Protein (MBP), Lymphocyte antigen 6B.2 (Ly-6B.2), Matrix Metalloproteinase-12 (MMP12), Mucin 5B (MUC5B), and Mucin 5AC (MUC5AC) was performed using procedure published previously (24, 32-34). Briefly, formalin-fixed, paraffin-embedded lung sections were deparaffinized with Citrisolv (2 × 5 min each) and were rehydrated with graded ethanol (100%, 95%, 70%, 30%, distilled water; 3 min each). For MBP and Ly-6B.2, antigen retrieval was performed using Proteinase K (sections incubated for 20 min at 37°C, followed by cooling to room temperature). For MMP-12, MUC5B, and MUC5AC, antigen retrieval was performed using a citrate buffer-based heat-induced antigen-retrieval method (heating slides in 10mM sodium citrate solution [with 0.05% Tween 20; pH 6.0] at 95-100°C for 30 min, followed by cooling to room temperature). Quenching for endogenous peroxidases was performed with 3% hydrogen peroxide in deionized water for 10 min at room temperature. Sections were blocked with the blocking buffer for 20 min followed by primary antibody incubation with rat monoclonal MBP primary antibody (MT-14.7.3; Mayo Clinic, Scottsdale, AZ), Ly-6B.2 (MCA771G; Clone 7/4, Bio-Rad, Hercules, CA), rabbit polyclonal to MMP-12 (ab66157; Abcam, Cambridge, MA), rabbit polyclonal MUC5B primary antibody (UNC223; University of North Carolina, Chapel Hill, NC), MUC5AC primary antibody (UNC294; University of North Carolina, Chapel Hill, NC)] at room temperature (RT) for 2 hours. Sections were washed and incubated with diluted biotinylated secondary antibodies for 1 hour at RT. The sections were then rinsed in deionized water (2 × 5 min each) and processed using VECTASTAIN Elite ABC HRP Kit (PK-6101, Vector Laboratories, Burlingame, CA), followed by chromogenic substrate conversion to insoluble colored precipitate using ImmPACT Nova RED HRP substrate Kit (SK-4800, Vector Laboratories, Burlingame, CA). After a rinse in tap water, sections were counterstained with Gill's Hematoxylin-I, rinsed in de-ionized water, dehydrated with graded alcohol solutions, and coverslipped with VectaMount mounting media (H-5000, Vector Laboratories, Burlingame, CA). Mounted slides were imaged using transmitted light microscopy (Nikon Ci-L microscope). Immunostained slides were analyzed for the determination of positively stained cells. Briefly, photographs were captured under 40X objective of the ECLIPSE Ci-L microscope with DS-Fi2 camera attachment (Nikon, Melville, NY). Thereafter, captured images were processed using the ImageJ software (NIH) to determine the percent positively stained area (MUC5B and MUC5AC) or positively stained cells (MMP12) (29).

Gene expression

Gene expression analyses on mRNA harvested from right lungs were performed as previously described (33).

Statistical analyses:

One-way Analysis of Variance (ANOVA) followed by Tukey's post hoc test for multiple comparisons was used to determine significant differences among groups. Outliers were removed using Grubb's test. Individual data point in scatter plots represents an individual animal. All data were expressed as mean ± standard error of the mean (SEM). To minimize the number of horizontal bars indicating statistically significant differences between experimental groups, we used a single bar when one group was significantly different than multiple other groups and used smaller vertical bars to indicate the groups that were being compared. P-value < 0.05 was considered statistically significant. Statistical analyses were performed using GraphPad Prism 8.0 (GraphPad Software, La Jolla, CA).

Results

Ozone exposure compromises body weight gain and increases the permeability of the epithelial-endothelial barrier in Scnn1b-Tg+ (Tg+) mice

To study the characteristics of ozone-induced lung disease in developing mice lungs in WT and in *Scnn1b*-Tg+ (Tg+) mice that manifest spontaneous mucoinflammatory lung disease with neonatal-onset (PND2-3 days), 3-day-old WT and *Scnn1b*-Tg+ neonates were exposed to filtered air (FA) or 800 ppb ozone until the age of 20 days and necropsied at PND21 (weaning age) (Fig. 1A). Neonates were exposed to a designated environment for 4 hours per day in nightly conditions and analyzed for designated endpoints including BALF immune cell composition, inflammatory mediator analysis, bacterial burden, immunoglobulins isotype determination, histopathological and immunohistochemical analyses, and gene expression analyses (Fig. 1A).

Bodyweight gain was comparable between FA-exposed WT (6.12 ± 0.27 g) and ozone-exposed WT (5.69 ± 0.38 g) mice (Fig. 1B). However, the body weight gain was significantly less in ozone-exposed *Scnn1b*-Tg+ (4.71 ± 0.27 g) versus FA-exposed *Scnn1b*-Tg+ (6.32 ± 0.18 g) mice (Fig. 1B). Ozone is known to cause injury to the gas exchange barrier which is indicated by the leakage of proteins into the alveolar airspaces (35, 36). To investigate the extent of injury to the gas exchange barrier in the developing neonates with and without *Scnn1b*-Tg+ lung disease, we assayed the total protein contents in the BALF from WT and *Scnn1b*-Tg+ mice exposed to either FA or ozone. The total protein contents were higher in ozone-exposed WT (267.9 ± 22.61 μg/ml) versus FA-exposed WT (187.9 ± 17.76 μg/ml) mice. The total protein contents in FA-exposed *Scnn1b*-Tg+ mice were 246.9 ± 23.32 μg/ml. Ozone exposure significantly increased the total protein in *Scnn1b*-Tg+ mice (571.3 ± 49.81 μg/ml; ~3-fold as compared FA-exposed WT mice; ~2.1-fold as compared to ozone-exposed WT mice; ~2.3-fold as compared FA-exposed *Scnn1b*-Tg+ mice) (Fig. 1C).

Increased levels of double-stranded (ds) DNA in the BALF are indicative of airway epithelial damage and inflammation (37, 38). To determine whether ozone exposure causes

an increase in BALF dsDNA, we assayed DNA contents in the BALF from WT and *Scnn1b*-Tg+ mice exposed to either FA or ozone. To our surprise, despite the presence of a mucoinflammatory lung disease in the *Scnn1b*-Tg+ neonates, FA-exposed *Scnn1b*-Tg+ neonates had dsDNA contents that were comparable to FA-exposed WT neonates (Fig. 1D). However, as expected, ozone exposure resulted in a significant increase in the dsDNA content in the BALF of WT as well as *Scnn1b*-Tg+ mice (Fig. 1D).

Ozone exposure disrupts the immune cell composition of the airspaces of WT and Scnn1b-Tg+ mice

To study immune cell recruitment in ozone-exposed neonates during active phases of postnatal lung development in WT and *Scnn1b*-Tg+ neonates with mucoinflammatory lung disease, we performed immune cell analyses of the BALF from FA- or ozone-exposed WT and *Scnn1b*-Tg+ mice. Ozone exposure resulted in a significant increase in total cell counts in ozone-exposed WT mice versus FA-exposed WT mice (Fig. 2A). This increase in total cell counts was attributable to significantly increased numbers of neutrophils, eosinophils, and lymphocytes (Fig. 2B-D). As reported previously (24), the FA-exposed *Scnn1b*-Tg^+ mice had significantly higher numbers of BALF immune cells (~3.1-fold versus FA-exposed WT mice, Fig. 2A), which was attributable to a significant increase in macrophage, neutrophil, eosinophil, and lymphocyte counts (Fig. 2B-D). Ozone exposed-*Scnn1b*-Tg^+ mice exhibited a significant increase in the total cell counts as compared to FA-exposed WT mice and ozone-exposed WT mice (Fig. 2A). Further, total cell counts were significantly higher in ozone-exposed *Scnn1b*-Tg^+ mice versus FA-exposed *Scnn1b*-Tg+ mice (Fig. 2A), which were attributed to a significant increase in neutrophils, eosinophils, and lymphocytes (Fig. 2B-D). A similar trend was observed when the lung sections were immunostained for major basic protein (MBP), an eosinophil specific marker, (Fig. 2E-F) and Ly-6B.2, neutrophil and inflammatory monocyte specific marker (Fig. 2E-F).

While only 0.1% of BALF macrophages from FA-exposed WT mice had surface area above 300μm^2, ~5.6% of macrophages had surface area greater than 300μm^2 in ozone-exposed WT mice (Supplemental Fig. 1). Further, the relative frequency of macrophages with 200μm^2 surface area was ~5% in FA-exposed WT mice versus ~19.5% in ozone-exposed WT mice. As previously reported (19, 34), BALF macrophages from *Scnn1b*-Tg^+ mice were morphologically activated. While ~12.6% of macrophages in FA-exposed *Scnn1b*-Tg^+ mice had surface area greater than 300μm^2, ~19.1% BALF macrophages were larger than 300μm^2 in ozone-exposed *Scnn1b*-Tg^+ mice (Supplemental Fig. 1). These data suggest that early postnatal ozone exposure enhances immune cell recruitment and morphological activation of macrophages in the lung airspaces of WT mice and that this response is further exaggerated in the presence of an existing/ongoing muco-obstructive airway disease.

Ozone exposure alters the levels of inflammatory mediators in the airspaces of WT and Scnn1b-Tg+ mice

We reasoned that the increased numbers of immune cells in the airspaces of ozone-exposed neonates are due to the elevated levels of chemokines in the airspaces, therefore, we assessed the levels of chemokines in the BALF from FA- and ozone-exposed WT and *Scnn1b*-Tg+ mice. First, we investigated the levels of primary neutrophil chemokines, including KC/

CXCL1, MIP-2 /CXCL2, MCP-1/CCL2, and G-CSF. KC/CXCL1 levels trended higher in ozone-exposed WT mice as compared to FA-exposed WT mice, but the increase was not statistically significant (Fig. 3A). As previously reported (17), KC levels were significantly higher in FA-exposed *Scnn1b*-Tg+ mice as compared to FA-exposed WT mice (Fig. 3A). FA-exposed *Scnn1b*-Tg+ mice also displayed significantly higher levels of KC as compared to ozone-exposed WT mice (Fig. 3A). Contrary to elevated neutrophil counts, the KC levels in ozone-exposed *Scnn1b*-Tg+ mice were significantly lower versus FA-exposed *Scnn1b*-Tg+ mice (Fig. 3A). As previously reported (19), FA-exposed *Scnn1b*-Tg+ mice showed significantly increased levels of MIP-2/CXCL2 as compared to FA-exposed WT mice (Fig. 3B). While there was a significant increase in MIP-2 levels in FA-exposed *Scnn1b*-Tg+ mice as compared to ozone-exposed WT mice, there was no difference in MIP-2 levels among other groups. MCP-1/CCL2, a chemokine for neutrophils as well as monocytes, was comparable among FA-exposed WT, ozone-exposed WT, and FA-exposed *Scnn1b*-Tg+ mice. The BALF levels for MCP-1 were, however, significantly elevated in ozone-exposed *Scnn1b*-Tg^{+} mice (~3.6-fold versus FA-exposed *Scnn1b*-Tg+ mice; ~5.5-fold versus ozone-exposed WT mice; ~5.5-fold versus FA-exposed WT) (Fig. 3C). Consistent with increased neutrophilic counts in ozone-exposed *Scnn1b*-Tg+ mice, the G-CSF levels in ozone-exposed *Scnn1b*-Tg+ mice were also significantly elevated (~11.7-fold as compared to ozone-exposed WT mice and ~60-fold versus FA-exposed WT mice, Fig. 3D).

Next, we investigated the levels of primary eosinophil chemokines, including CCL5 (Rantes) (Fig. 3E), CCL7 (MCP3) (Fig. 3F), CCL11 (Eotaxin-1) (Fig. 3G), CCL12 (MCP5) (Fig. 3H), CCL17 (Fig. 3I), CCL22 (Fig. 3J), CCL24 (Eotaxin-2) (Fig. 3K). Except for CCL17, none of these chemokines were significantly elevated in ozone-exposed WT or FA-exposed *Scnn1b*-Tg+ mice. As compared to FA-exposed WT, while the mean concentration of CCL17 was insignificantly increased in ozone-exposed WT mice, the FA-exposed *Scnn1b*-Tg+ had significantly higher levels of CCL17 (Fig. 3I). Except for CCL5 (Fig. 3E), all the eosinophil chemokines (Fig. 3F-K) were significantly elevated in ozone-exposed *Scnn1b*-Tg+ mice.

Expression levels of MIP-1α/CCL3, another chemokine for macrophages, lymphocytes, eosinophils, and neutrophils trended higher in ozone-exposed WT mice versus FA-exposed WT mice but the difference was not significant. Consistent with the significant increase in macrophage, lymphocyte, eosinophil, and neutrophils counts, MIP-1α levels were significantly increased in FA-exposed *Scnn1b*-Tg+ mice (~8.9-fold versus FA-exposed WT mice, Fig. 3L). Although ozone-exposed *Scnn1b*-Tg+ and ozone-exposed WT mice showed comparable macrophage as well as eosinophil counts, the significant increase in MIP-1α in ozone-exposed *Scnn1b*-Tg+ (~5.4-fold versus ozone-exposed WT, Fig. 3L) might in part contribute to increased neutrophil and lymphocyte recruitment in this group (Fig. 2 B-C). The expression level of MIP-1α was comparable among ozone-exposed *Scnn1b*-Tg+ and FA-exposed *Scnn1b*-Tg+ mice.

MIP-1β/CCL4, a chemokine for monocytes, eosinophils, and lymphocytes, was comparable among ozone-exposed WT versus FA-exposed WT mice. FA-exposed *Scnn1b*-Tg+ mice showed significantly increased MIP-1β levels as compared to FA-exposed WT mice (~8.5-fold, Fig. 3M) which mirrored the significant increase in macrophages, eosinophils, and

lymphocytes in this group. While MIP-1β levels trended higher in ozone-exposed *Scnn1b*-Tg+ mice as compared to FA-exposed *Scnn1b*-Tg+ mice, the difference was not statistically significant. IL-6 and IP-10 (CXCL10), both consistently found in ozone-exposed airspaces, were significantly upregulated in the ozone-exposed *Scnn1b*-Tg+ mice (Fig. 3N-O).

Ozone exposure worsens parenchymal pathology in WT and Scnn1b-Tg+ mice

Next, the effects of ozone exposure on the parenchymal morphology and alterations associated with the inflammatory changes in WT and *Scnn1b*-Tg+ mice were evaluated. FA-exposed WT mice had no signs of the infiltration of immune cells around pulmonary vessels (perivascular inflammation) or in and around the intrapulmonary airways (peribronchiolar inflammation) (Fig. 4A, E, I), alveolar space enlargement (Fig. 4B, E, I), lymphoid hyperplasia (Fig. 4C, E, I), and increase in the thickness of the alveolar septa/infiltration of alveolar spaces with inflammatory cells (septal thickening/consolidation) (Fig. 4D, E, I). In contrast, the ozone-exposed WT mice exhibited marked signs of perivascular and peribronchiolar inflammation (Fig. 4A, F, M), alveolar space enlargement (Fig. 4B, F, J), and septal thickening/consolidation (Fig. 4D, F, M).

As previously reported (24), FA-exposed *Scnn1b*-Tg+ mice had significant perivascular and peribronchiolar inflammation (Fig. 4A, G, N), alveolar space enlargement (Fig. 4B, G, K), lymphoid hyperplasia (Fig. 4C, G, N), and septal thickening/consolidation (Fig. 4D, G, N). As compared to FA-exposed *Scnn1b*-Tg+ mice, the ozone-exposed *Scnn1b*-Tg+ mice had significant perivascular and peribronchiolar inflammation (Fig. 4A, H, O, P), alveolar space enlargement (Fig. 4B, H, L), and septal thickening/consolidation (Fig. 4D, H, O, P). Despite the relatively larger size of lymphoid aggregates in ozone-exposed *Scnn1b*-Tg+ mice, the incidence of lymphoid aggregates was comparable between FA-exposed and ozone-exposed *Scnn1b*-Tg+ mice (Fig. 4C, P).

MMP12, matrix metalloproteinase-12, is a critical protease in the pathogenesis of emphysema in various disease models including *Scnn1b*-Tg+ mice (39-41). To determine whether the emphysematous responses in the three experimental groups are caused by the upregulated expression of MMP12, we assessed MMP12 protein contents and *Mmp12* mRNA levels in the lungs of these mice. The MMP12 stained cells were scarce in FA-exposed WT mice but widespread in the lungs from the three groups with alveolar space enlargement (Fig. 5A-B). Among the three groups with increased MMP12+ cell counts, only ozone-exposed *Scnn1b*-Tg+ mice had significantly higher MMP12+ cell counts versus FA-exposed WT mice (Fig. 5B). While macrophage staining intensity was comparable between FA-exposed *Scnn1b*-Tg+ and ozone-exposed *Scnn1b*-Tg+ mice (Fig. 5A), macrophages were morphologically enlarged in ozone-exposed *Scnn1b*-Tg+ versus FA-exposed *Scnn1b*-Tg+ mice (Supplemental Fig. 1). This suggests that macrophages are morphologically activated and may contribute towards relatively greater MMP12 activity, and resultingly exaggerated alveolar space enlargement in ozone-exposed *Scnn1b*-Tg+ mice (Fig. 5A-B). Consistent with MMP12 immunostaining, as compared to the FA-exposed WT mice, the *Mmp12* mRNA levels were increased in both ozone-exposed WT and FA-exposed *Scnn1b*-Tg+ mice but the differences were not statistically significant (Fig. 5C). The ozone-exposed

Scnn1b-Tg+ mice had significantly higher expression of *Mmp12* mRNA as compared to FA-exposed *Scnn1b*-Tg+ mice (Fig. 5C).

Ozone exposure induces the expression of Type 2 inflammation-associated gene signatures in WT and Scnn1b-Tg+ mice

Ozone inhalation causes epithelial remodeling with Type 2 immune response in the airways of adult mice (26, 32, 42), and Type 2 responses have been previously reported in the *Scnn1b*-Tg+ mice (24, 43). To determine the effect of ozone exposure on epithelial remodeling in developing lungs of WT and *Scnn1b*-Tg+ mice, we analyzed the levels of soluble mediators in the BALF and the expression of genes that are known to drive Type 2 inflammatory responses in the lung.

First, we analyzed the mRNA expression levels of the three master regulators of Type 2 immunity, i.e., *Il33, Tslp, and Il25*. As compared to FA-exposed WT mice, the ozone-exposed WT mice had upregulated levels of mRNAs for *Il33* ($p<0.05$; Fig. 6A) as well as *Tslp* ($p=0.07$; Fig. 6B). Although the FA-exposed *Scnn1b*-Tg+ mice had an elevated level of mRNAs for *Il33* as well as *Tslp* as compared to FA-exposed WT mice, the upregulation was not statistically significant. As compared to FA-exposed *Scnn1b*-Tg+ mice, the ozone-exposed *Scnn1b*-Tg+ mice had increased levels of *Il33* mRNA and *Tslp* mRNA but the difference was not statistically significant. Although the *Il25* mRNA was not detected in all the samples analyzed, the comparison of mean expression in those samples in which it was detected revealed higher levels in ozone-exposed WT as well as ozone-exposed *Scnn1b*-Tg+ mice (Fig. 6C). Following the *Il33* mRNA trend, IL-33 protein levels were elevated in both ozone-exposed WT and *Scnn1b*-Tg+ mice (Fig. 6D).

Next, we analyzed protein and mRNA levels of primary Type 2 cytokines, i.e., IL-4, IL-13, and IL-5 in all four experimental groups. IL-4 contents trended higher in the BALF from ozone-exposed WT (1.13 ± 0.24 pg/ml) versus FA-exposed WT (0.55 ± 0.016 pg/ml) mice (Fig. 6E). Consistent with the cytokine contents, the *Il4* mRNA levels also trended higher in ozone-exposed WT versus FA-exposed WT mice (Fig. 6F). As compared to FA-exposed WT mice, FA-exposed *Scnn1b*-Tg+ mice had elevated levels of both IL-4 protein (Fig. 6E**; $p<0.001$**) and *Il4* mRNA (Fig. 6F**, not significant**). While the IL-4 protein contents were comparable between FA- and ozone-exposed *Scnn1b*-Tg+ mice (Fig. 6E), the ozone-exposed *Scnn1b*-Tg+ mice had significantly elevated levels of *Il4* mRNA (Fig. 6F).

IL-13 protein levels (Fig. 6G) and *Il13* mRNA (Fig. 6H) were comparable among ozone-exposed WT versus FA-exposed WT mice but trended higher in FA-exposed *Scnn1b*-Tg+ mice. IL-13 protein contents were significantly elevated (Fig. 6G) while *Il13* mRNA levels trended higher (Fig. 6H**; $p=0.07$**) in ozone-exposed *Scnn1b*-Tg+ versus FA-exposed *Scnn1b*-Tg+ mice.

IL-5 is a key Type 2 cytokine that plays a key role in the proliferation, maturation, differentiation, and migration of eosinophils (44-46). IL-5 protein levels trended higher in ozone-exposed WT versus FA-exposed WT mice and FA-exposed *Scnn1b*-Tg+ versus FA-exposed WT but the differences were not statistically significant (Fig. 6I). Consistent with the presence of increased numbers of eosinophils in ozone-exposed *Scnn1b*-Tg+ mice

(Fig. 2), IL-5 levels were significantly higher in ozone-exposed *Scnn1b*-Tg+ mice (~3.1-fold versus FA-exposed *Scnn1b*-Tg+; ~12.4-fold versus ozone-exposed WT mice; ~196.7-fold versus FA-exposed WT mice, Fig. 6I). The *Il5* mRNA levels trended higher in ozone-exposed WT, FA-exposed *Scnn1b*-Tg+, and ozone-exposed *Scnn1b*-Tg+ mice compared to FA-exposed WT mice (Fig. 6J).

Ozone exposure promotes mucoinflammatory responses in WT and Scnn1b-Tg+ mice

Airway mucus obstruction is a consistent feature of *Scnn1b-Tg+* lung disease (17). To investigate the role of ozone in modulating mucus obstruction, we assessed the airway luminal mucus contents in AB-PAS stained lung sections from WT and *Scnn1b*-Tg+ mice exposed to FA or ozone. While the FA-exposed WT mice had no signs of mucous cell metaplasia and airway mucus obstruction (Fig. 7A, B), the airways from ozone-exposed WT mice had a marked increase in the proportion of mucous cells and the degree of airway mucus obstruction (Fig. 7A, B). As previously reported (24), FA-exposed *Scnn1b*-Tg+ mice had elevated numbers of mucous cells associated with airway mucus obstruction (Fig. 7A, B). Ozone exposure to *Scnn1b*-Tg+ mice, however, significantly increased the degree of airway mucus obstruction (Fig. 7A, B)

Airway mucus obstruction in *Scnn1b-Tg+* mice is primarily contributed by two gel-forming mucins, i.e., MUC5B and MUC5AC. To determine the effect of ozone exposure on the expression of these mucins and their contribution to the mucus obstruction, we quantified the mRNA expression for *Muc5b* (Fig. 7C) and *Muc5ac* (Fig. 7F) in total mRNA collected from lungs as well as performed immunolocalization of MUC5B (Fig. 7D-E) and MUC5AC (Fig. 7G-H) in lung sections. The mRNA levels for *Muc5b* were minimal in FA-exposed WT mice. The *Muc5b* mRNA levels were significantly elevated in ozone-exposed WT as well as FA-exposed *Scnn1b*-Tg+ mice. The epithelial immunostaining intensity for MUC5B (Fig. 7D-E) was consistent with their mRNA levels (Fig. 7C). Importantly, while the *Muc5b* mRNA levels were comparable between FA-exposed and ozone-exposed *Scnn1b*-Tg+ mice, the intraluminal staining was more widespread in ozone-exposed *Scnn1b*-Tg+ mice which is consistent with the significantly greater airway mucus obstruction in ozone-exposed *Scnn1b*-Tg+ mice (Fig. 7D). The percent area stained positively for MUC5B intracellular immunostaining were significantly increased in ozone-exposed WT versus FA-exposed WT, FA-exposed *Scnn1b*-Tg+ versus ozone-exposed WT and, ozone-exposed Scnn1b-Tg+ mice versus FA-exposed *Scnn1b*-Tg+ mice (Fig. 7E).

As compared to the FA-exposed WT mice, *Muc5ac* mRNA levels were significantly elevated in the ozone-exposed WT mice (Fig. 7F). Consistent with the mRNA levels, the MUC5AC immunostaining was widespread in the airways of ozone-exposed WT mice compared to FA-exposed WT mice (Fig. 7G-H). As compared to FA-exposed *Scnn1b*-Tg+ mice, the *Muc5ac* mRNA levels trended higher in ozone-exposed *Scnn1b*-Tg+ mice (Fig. 7F). Consistent with this, the relative proportion of MUC5AC stained cells was higher in the ozone-exposed *Scnn1b*-Tg+ versus FA-exposed *Scnn1b*-Tg+ mice (Fig. 7H). These data suggest that MUC5AC is upregulated in the presence of ozone or airway surface liquid dehydration but the superimposition of ozone exposure onto the airway surface liquid dehydration does not have any synergistic or additive effect.

Next, we performed gene expression analyses for genes including *Spdef* (Fig. 7I), *Foxa2* (Fig. 7J), *Agr2* (Fig. 7K), *Slc26a4* (Fig. 7L), *Retnla* (Fig. 7M), and *Chil4* (Fig. 7N) that are known to be associated with mucus production and Type 2 inflammation. As compared to the FA-exposed WT mice, the ozone-exposed WT mice had a higher expression for all the assayed genes, but a significant difference was attained only for *Retnla and Chil4* (Fig. 7M-N). In contrast to WT mice, the effect of ozone exposure was more pronounced in *Scnn1b*-Tg+ mice. As compared to the FA-exposed *Scnn1b*-Tg+ mice, the ozone-exposed *Scnn1b*-Tg+ mice had a significantly higher expression for all the assayed genes, except *Foxa2* (Fig. 7J)> *and Chi4* (Fig. 7N).

Ozone exposure reduces bacterial clearance in Scnn1b-Tg+ mice

Due to mucociliary clearance defect, the *Scnn1b*-Tg+ mice are prone to spontaneous bacterial infections arising from the aspiration of bacteria of oropharyngeal origin, that usually clear up by 3-4 weeks of age (19). To determine the effect of ozone exposure on the clearance of bacterial infections, we analyzed the bacterial burden in aseptically harvested BALF from FA- or ozone-exposed WT and *Scnn1b*-Tg+ mice. Only 13% of FA-exposed WT mice (3 out of 23; mean CFU~8.7/ml) and 20% of ozone-exposed WT mice (3 out of 15; mean CFU ~15.6/ml) exhibited mild bacterial infection. As expected from previous studies, 34.6% (9 out of 26 mice; CFU~82.7/ml) of FA-exposed *Scnn1b*-Tg+ mice still had bacterial infection (mean CFU~82.7/ml) at postnatal day 21. In contrast, 75% (15 out of 20 mice) of ozone-exposed *Scnn1b*-Tg+ mice displayed significantly higher bacterial infection with a mean CFU ~725/ml (Fig. 8A).

Ozone exposure induced reduced bacterial clearance in Scnn1b-Tg+ mice is associated with elevated IL-10

IL-10, an immunosuppressive and anti-inflammatory cytokine, was recently shown to suppress bacterial clearance in *Scnn1b*-Tg+ mice (43). To determine whether the reduced bacterial clearance in ozone-exposed *Scnn1b*-Tg+ mice is associated with IL-10 overproduction, we analyzed IL-10 protein levels in BALF and *Il10* mRNA levels in lung homogenates. *Il10* mRNA levels were comparable in the lungs from FA-exposed, ozone-exposed WT, and FA-exposed *Scnn1b*-Tg+ mice. Interestingly, the ozone-exposed *Scnn1b*-Tg+ mice had significantly increased levels of *Il10* mRNA (Fig. 8B). Consistent with the mRNA levels, the BALF IL-10 levels were comparable in FA-exposed WT, ozone-exposed WT, and FA-exposed *Scnn1b*-Tg+ mice whereas the BALF levels of IL-10 were elevated in ozone-exposed *Scnn1b*-Tg+ mice (Fig. 8C).

Ozone exposure increases the production of immunoglobulins

Ozone has been shown to compromise the immunoglobulin production by B-cells *in vitro* (47). Accordingly, we speculated that the immunoglobulin-mediated bacterial clearance defense system may have been compromised in ozone-exposed *Scnn1b*-Tg+ mice. Therefore, we assayed the levels of immunoglobulins (IgA, IgG1, IgG2a, IgG2b, IgG3, IgM) in the BALF from FA- and ozone-exposed WT and *Scnn1b*-Tg+ mice. IgA was found elevated only in the BALF from FA-exposed *Scnn1b*-Tg+ mice versus all the other groups (Fig. 8D). IgG1 was not different among any of the groups (Fig. 8E). Three isotypes of IgG, i.e., IgG2a, IgG2b, IgG3, were significantly elevated in BALF from ozone-exposed

WT mice versus FA-exposed WT (Fig. 8F-H). Although the mean concentration values for IgG isotypes were higher in FA-exposed *Scnn1b*-Tg+ mice versus FA-exposed WT mice, the differences were not statistically significant (Fig. 8F-H). The concentration of both IgG2b and IgG3 were significantly elevated in ozone-exposed *Scnn1b*-Tg+ versus FA-exposed *Scnn1b*-Tg+ mice (Fig. 8G-H). As compared to FA-exposed WT mice, both ozone-exposed WT and FA-exposed *Scnn1b*-Tg+ mice had elevated levels of IgM, but the differences were not statistically significant (Fig. 8I). The levels of IgM were significantly elevated in ozone-exposed *Scnn1b*-Tg+ as compared to FA-exposed *Scnn1b*-Tg+ mice (Fig. 8I). In summary, except for IgA, where a trend for lower concentration was observed in ozone-exposed *Scnn1b*-Tg+ (10.1 ± 1.47 ng/ml) versus FA-exposed *Scnn1b*-Tg+ (16.9 ± 4.47 ng/ml) mice, all the other immunoglobulin subtypes were present at elevated levels (Fig. 8E-I) in ozone-exposed *Scnn1b*-Tg+ mice versus FA-exposed *Scnn1b*-Tg+ mice. In particular, IgG2b, IgG3, and IgM were significantly elevated in ozone-exposed *Scnn1b*-Tg+ mice versus FA-exposed *Scnn1b*-Tg+ mice (Fig. 8G-I). These results indicate that reduced bacterial clearance in *Scnn1b*-Tg+ mice following ozone exposure is not attributed to reduced production of immunoglobulins.

Discussion:

A significant knowledge gap exists in our understanding of the interactions between ozone-dominated air pollution, early postnatal lung development, and pathogenesis of mucoinflammatory lung diseases of genetic origin. Cystic Fibrosis (CF), a genetic disease caused by a gene mutation in the CFTR gene, initiates during early childhood, and mucoinflammatory lung disease in CF patients contributes to significant morbidity and mortality (48). Our PubMed search for the interaction between ozone and cystic fibrosis found only three studies that reported the association between ozone exposure and pulmonary exacerbations in CF patients (7, 8, 25). Experimental *in vivo* studies investigating the three-dimensional interaction between inhaled ozone, lung development, and disease pathogenesis have never been performed. Accordingly, this mouse-based study was conceived to address two key questions: 1) Does ozone affect the normal lung development in wildtype (WT) neonates? 2) Does ozone affect the developmental history of CF-like mucoinflammatory lung disease in mice?

In WT mice, ozone exposure resulted in a significant disruption in lung development, both morphologically and in terms of inflammatory responses. For instance: 1) the increase in the proportions of AB-PAS-positive, MUC5AC-positive, MUC5B-positive mucous cells following ozone exposure reflected significant airway epithelial remodeling, 2) Increased proportion of mucous cells possibly resulted in mucus obstruction of the airways post ozone exposure, 3) Alveolar space enlargement (emphysema) was prominent in ozone-exposed WT mice, 4) Granulocytic (neutrophilic and eosinophilic) inflammation in airspaces as well as in subepithelial regions was established following ozone exposure, 5) Gene signatures of Type 2 inflammation, including *Il33, Tslp, Il5, Muc5b, Muc5ac, Retnla, and Chil4* were upregulated following ozone exposure. 6) IgG immunoglobulin subtypes including IgG2a, IgG2b, and IgG3, were significantly elevated in the BALF following ozone exposure. These outcomes indicate a marked impact of ozone on postnatal lung development and in the establishment of Type 2 inflammatory disease. However, it remains to be tested whether

these pathological features are reversible and whether these early life ozone exposures affect respiratory health during adulthood.

In CF infants, the clinical signatures of neutrophil-dominated airway inflammation are present within the first few weeks of life (49, 50). Bacterial infections have been reported in CF infants as early as 3 months of age (51). Structural changes, i.e., bronchiectasis and air trapping become evident during preschool years, in particular, between 3-5 years of age (52, 53). During the first 3 years of life, a period critical for the alveolar maturation phase of lung development (54), most of the pathological features of the CF lung disease are well established. The *Scnn1b*-Tg+ mice, a widely accepted model of cystic fibrosis, exhibit clinical signatures of human CF-like lung disease including early postnatal initiation of airway mucus obstruction, airway surface liquid dehydration, granulocytic airway inflammation, and spontaneous bacterial infection within the first 21 days of their life (17, 19). Accordingly, we exposed *Scnn1b*-Tg+ neonates to ozone beginning at post-natal day 3 until the age of 20 days, which corresponds to early preschool years (55).

Ozone exposure to the *Scnn1b*-Tg+ mice resulted in a significant worsening of most of the mucoinflammatory features that are inherent to this model (17). For instance: 1) granulocytic (neutrophilic and eosinophilic) recruitment to *Scnn1b*-Tg+ lungs was significantly increased, 2) a large number of inflammatory mediators were present at significantly higher levels, 3) bacterial clearance was compromised, 4) alveolar space enlargement was severe, and 5) mucus obstruction and associated MUC5B protein expression was significantly higher. Putting together data from ozone-exposed WT and *Scnn1b*-Tg+ mice, it appears that the ozone and airway surface liquid (ASL) dehydration independently initiate Type 2 inflammatory cascades. Further, the superimposition of the two stresses exaggerates the Type 2 mucoinflammatory features.

MMP12, a matrix metalloproteinase, has been implicated in alveolar wall destruction resulting in alveolar space enlargement, also known as emphysema (39, 40). Ozone-exposed WT mice had widespread alveolar space enlargement. Alveolar space enlargement, a consistent feature in *Scnn1b*-Tg+ mice (17), was marked in FA-exposed *Scnn1b*-Tg+ mice. In both of these groups, i.e., ozone-exposed WT and FA-exposed *Scnn1b*-Tg+ mice, *Mmp12* mRNA and protein levels were elevated. Further, the superimposition of ozone exposure on *Scnn1b*-Tg+ lung disease caused further enlargement of alveolar spaces that was associated with increased mRNA and protein expression of MMP12. Based on a previous report that demonstrated macrophage-specific MMP12 expression in *Scnn1b*-Tg+ mice is involved in alveolar space enlargement (41), ozone appears to induce MMP12 expression in activated macrophages that initiates alveolar space enlargement in WT mice and exaggerate this feature in *Scnn1b*-Tg+ mice. In addition to MMP12, neutrophil elastase (NE) has also been implicated in alveolar space enlargement in *Scnn1b*-Tg+ mice (56). Given significant neutrophilic inflammation in ozone-exposed WT mice, FA-exposed *Scnn1b*-Tg+, and ozone-exposed *Scnn1b*-Tg+ mice, the contribution of neutrophil-derived NE towards alveolar space enlargement cannot be ruled out. Whether both or one of the two proteases, i.e., macrophage-derived MMP12 or neutrophil-derived NE contribute to emphysema, however, remains untested.

The *Scnn1b*-Tg+ mice are prone to spontaneous bacterial infections that usually clear up by 3-4 weeks of age (19). Interestingly, while only ~35% of the FA-exposed *Scnn1b*-Tg+ mice had bacterial infection (CFU ~82.7/ml), nearly 75% of the ozone-exposed *Scnn1b*-Tg+ mice still had bacterial infection (CFU ~725/ml) indicating an effect of ozone on bacterial clearance. Delayed bacterial clearance has also been reported in *Scnn1b*-Tg+ mice that were either exposed to secondhand smoke (24) or were functionally or numerically deficient in immune cells (18, 43). In these studies, various factors including compromised immune cell function or exaggerated mucus obstruction were suggested as the contributors to sustained bacterial infections. In the current study, IL-10, a known suppressor of the antibacterial function of macrophages in *Scnn1b*-Tg+ mice (43), was found to be significantly elevated in ozone-exposed *Scnn1b*-Tg+ mice. Mucus obstruction, another factor favoring bacterial colonization, was also more widespread in the ozone-exposed *Scnn1b*-Tg+ mice. Therefore, it is likely that these two factors, i.e., elevated IL-10 and the static mucus, a known fertile niche for bacterial growth, contributed to the persistence of bacterial infection in ozone-exposed *Scnn1b*-Tg+ mice. Their relative contribution towards defective bacterial clearance, however, remains to be tested. Interestingly, the immunoglobulin levels as well as neutrophils were sufficient and, in fact, increased in ozone-exposed *Scnn1b*-Tg^{+} mice, further suggesting that the compromised bacterial clearance was a result of mucus obstruction-induced mucociliary clearance defect rather than the compromised functioning of immunoglobulin-mediated or phagocyte-mediated bacterial clearance mechanisms.

Eosinophil-dominated inflammatory responses to subchronic levels of ozone exposure have been reported in adult mice (26, 32, 42). However, the nature of ozone-induced inflammatory response during the active phase of postnatal lung development has never been explored. Eosinophils, both within the BALF fluid and the lung tissue, were markedly increased following ozone exposure in WT mice, which were also associated with increases in the levels of mRNAs for Type 2 inflammation-associated cytokines, i.e., *Il33, Tslp,* and *Il5*. The superimposition of ozone exposure onto the preexisting *Scnn1b*-Tg+ lung disease further promoted Type 2 responses including BALF and tissue eosinophilia, *Il4* and *Il13* mRNA levels, and BALF IL-5, and IL-13 protein levels. Eosinophil chemokines including CCL7 (MCP3), CCL11 (Eotaxin-1), CCL12 (MCP5), CCL17, CCL22, and CCL24 (Eotaxin-2) were also significantly increased in ozone-exposed *Scnn1b*-Tg+ mice. Further, Type 2 inflammatory gene signatures including *Retnla* (Fizz1), *Chil4* (YM2), *Slc26a4* (Pendrin), and *Mmp12* were also significantly elevated following ozone exposure in either (WT or *Scnn1b*-Tg+) or both WT and *Scnn1b*-Tg+ mice. Based on previous reports (26, 42, 43), it could be speculated that these pronounced Type 2 responses are mediated through IL-33/TSLP→ILC2 axis, however, direct experimental testing of this conceptual model (Fig 8J) in neonates is awaited.

MUC5B and MUC5AC are prominent gel-forming mucins in the *Scnn1b*-Tg+ mucus plugs (57). The genetic ablation of MUC5B, but not MUC5AC, results in significantly reduced mucus obstruction in *Scnn1b*-Tg+ mice (57) suggesting a close association between the expression levels of MUC5B and the severity of mucus obstruction. We have previously reported reduced MUC5AC expression but sustained MUC5B expression and airway mucus obstruction in IL-33 knockout *Scnn1b*-Tg+ mice (33). Further, our recent study demonstrated that the ablation of innate lymphoid cells results in suppressed MUC5B

expression and diminished airway mucus obstruction (43). Based on these reports, the significantly increased mucus obstruction in ozone-exposed *Scnn1b*-Tg+ mice is most likely caused by a significant increase in airway MUC5B expression. However, the primary driver of increased MUC5B expression remains elusive.

While the current exposure paradigm revealed several interesting findings, some intriguing questions have also surfaced such as 1) How would the various exposure parameters, i.e., ozone dose and exposure time (single versus repeated) affects the outcome of various features of lung disease? 2) How would ozone exposure impact the clearance of experimentally-introduced bacteria in the lungs of WT and *Scnn1b*-Tg+ mice? 3) What is the effect of ozone exposure on the phagocytic functions of macrophages and macrophage recruitment? Future studies addressing these critical questions are warranted.

In conclusion, this study revealed interesting interactions between two independent airspace stressors, i.e., ozone and airway surface liquid dehydration. While both of these insults initiate Type 2 mucoinflammatory lung responses along a common axis, i.e., IL-33/TSLP→ILC2→MCM, the degree of mucoinflammatory features is more pronounced in *Scnn1b*-Tg+ mice. The superimposition of ozone onto CF-like *Scnn1b*-Tg+ lung disease results in exaggerated pulmonary pathology including Type 2 inflammation, persisted bacterial infection, mucus obstruction, and alveolar space enlargement. Based on these key findings, we propose that ozone exposure promotes pulmonary expression and secretion of IL-33 and/or TSLP that in turn orchestrates a series of Type 2 responses (Fig. 8J).

Supplementary Material

Refer to Web version on PubMed Central for supplementary material.

Acknowledgments

We thank Sherry Ring for histological tissue processing. We thank Thaya Stoufflet for assistance with multiplex cytokine assays. We thank Dr. Camille Ehre (University of North Carolina at Chapel Hill) for providing MUC5B and MUC5AC antibodies.

Funding:

This work was supported by the National Institute of General Medical Sciences Grant P20GM130555 (to Y.S.), and the National Institute of Environmental Health Sciences Grant R01ES030125 (to Y.S.).

References

1. Tager IB, Balmes J, Lurmann F, Ngo L, Alcorn S, and Kunzli N. 2005. Chronic exposure to ambient ozone and lung function in young adults. Epidemiology 16: 751–759. [PubMed: 16222164]
2. Kim CS, Alexis NE, Rappold AG, Kehrl H, Hazucha MJ, Lay JC, Schmitt MT, Case M, Devlin RB, Peden DB, and Diaz-Sanchez D. 2011. Lung function and inflammatory responses in healthy young adults exposed to 0.06 ppm ozone for 6.6 hours. Am J Respir Crit Care Med 183: 1215–1221. [PubMed: 21216881]
3. Dimakopoulou K, Douros J, Samoli E, Karakatsani A, Rodopoulou S, Papakosta D, Grivas G, Tsilingiridis G, Mudway I, Moussiopoulos N, and Katsouyanni K. 2020. Long-term exposure to ozone and children's respiratory health: Results from the RESPOZE study. Environ Res 182: 109002. [PubMed: 31855698]

4. Fauroux B, Sampil M, Quenel P, and Lemoullec Y. 2000. Ozone: a trigger for hospital pediatric asthma emergency room visits. Pediatr Pulmonol 30: 41–46. [PubMed: 10862161]
5. Lin S, Liu X, Le LH, and Hwang SA. 2008. Chronic exposure to ambient ozone and asthma hospital admissions among children. Environ Health Perspect 116: 1725–1730. [PubMed: 19079727]
6. Akinbami LJ, Lynch CD, Parker JD, and Woodruff TJ. 2010. The association between childhood asthma prevalence and monitored air pollutants in metropolitan areas, United States, 2001-2004. Environ Res 110: 294–301. [PubMed: 20117766]
7. Farhat SCL, Almeida MB, Silva-Filho L, Farhat J, Rodrigues JC, and Braga ALF. 2013. Ozone is associated with an increased risk of respiratory exacerbations in patients with cystic fibrosis. Chest 144: 1186–1192. [PubMed: 23493973]
8. Goss CH, Newsom SA, Schildcrout JS, Sheppard L, and Kaufman JD. 2004. Effect of ambient air pollution on pulmonary exacerbations and lung function in cystic fibrosis. Am J Respir Crit Care Med 169: 816–821. [PubMed: 14718248]
9. Strosnider HM, Chang HH, Darrow LA, Liu Y, Vaidyanathan A, and Strickland MJ. 2019. Age-Specific Associations of Ozone and Fine Particulate Matter with Respiratory Emergency Department Visits in the United States. Am J Respir Crit Care Med 199: 882–890. [PubMed: 30277796]
10. Khatri SB, Holguin FC, Ryan PB, Mannino D, Erzurum SC, and Teague WG. 2009. Association of ambient ozone exposure with airway inflammation and allergy in adults with asthma. J Asthma 46: 777–785. [PubMed: 19863280]
11. Zhang JJ, Wei Y, and Fang Z. 2019. Ozone Pollution: A Major Health Hazard Worldwide. Front Immunol 10: 2518. [PubMed: 31736954]
12. Salvi S 2007. Health effects of ambient air pollution in children. Paediatr Respir Rev 8: 275–280. [PubMed: 18005894]
13. Suwanwaiphatthana W, Ruangdej K, and Turner-Henson A. 2010. Outdoor air pollution and children's health. Pediatr Nurs 36: 25–32. [PubMed: 20361442]
14. Lewis BW, Patial S, and Saini Y. 2019. Immunopathology of Airway Surface Liquid Dehydration Disease. J Immunol Res 2019: 2180409. [PubMed: 31396541]
15. Clarke LL, Grubb BR, Yankaskas JR, Cotton CU, McKenzie A, and Boucher RC. 1994. Relationship of a non-cystic fibrosis transmembrane conductance regulator-mediated chloride conductance to organ-level disease in Cftr(−/−) mice. Proc Natl Acad Sci U S A 91: 479–483. [PubMed: 7507247]
16. Mall M, Grubb BR, Harkema JR, O'Neal WK, and Boucher RC. 2004. Increased airway epithelial Na+ absorption produces cystic fibrosis-like lung disease in mice. Nat Med 10: 487–493. [PubMed: 15077107]
17. Mall MA, Harkema JR, Trojanek JB, Treis D, Livraghi A, Schubert S, Zhou Z, Kreda SM, Tilley SL, Hudson EJ, O'Neal WK, and Boucher RC. 2008. Development of chronic bronchitis and emphysema in beta-epithelial Na+ channel-overexpressing mice. Am J Respir Crit Care Med 177: 730–742. [PubMed: 18079494]
18. Saini Y, Wilkinson KJ, Terrell KA, Burns KA, Livraghi-Butrico A, Doerschuk CM, O'Neal WK, and Boucher RC. 2016. Neonatal Pulmonary Macrophage Depletion Coupled to Defective Mucus Clearance Increases Susceptibility to Pneumonia and Alters Pulmonary Immune Responses. Am J Respir Cell Mol Biol 54: 210–221. [PubMed: 26121027]
19. Livraghi-Butrico A, Kelly EJ, Klem ER, Dang H, Wolfgang MC, Boucher RC, Randell SH, and O'Neal WK. 2012. Mucus clearance, MyD88-dependent and MyD88-independent immunity modulate lung susceptibility to spontaneous bacterial infection and inflammation. Mucosal Immunol 5: 397–408. [PubMed: 22419116]
20. Seys LJ, Verhamme FM, Dupont LL, Desauter E, Duerr J, Seyhan Agircan A, Conickx G, Joos GF, Brusselle GG, Mall MA, and Bracke KR. 2015. Airway Surface Dehydration Aggravates Cigarette Smoke-Induced Hallmarks of COPD in Mice. PLoS One 10: e0129897. [PubMed: 26066648]
21. Geiser M, Wigge C, Conrad ML, Eigeldinger-Berthou S, Kunzi L, Garn H, Renz H, and Mall MA. 2014. Nanoparticle uptake by airway phagocytes after fungal spore challenge in murine allergic asthma and chronic bronchitis. BMC Pulm Med 14: 116. [PubMed: 25027175]

22. Geiser M, Quaile O, Wenk A, Wigge C, Eigeldinger-Berthou S, Hirn S, Schaffler M, Schleh C, Moller W, Mall MA, and Kreyling WG. 2013. Cellular uptake and localization of inhaled gold nanoparticles in lungs of mice with chronic obstructive pulmonary disease. Part Fibre Toxicol 10: 19. [PubMed: 23680060]
23. Jia J, Conlon TM, Ballester Lopez C, Seimetz M, Bednorz M, Zhou-Suckow Z, Weissmann N, Eickelberg O, Mall MA, and Yildirim AO. 2016. Cigarette smoke causes acute airway disease and exacerbates chronic obstructive lung disease in neonatal mice. Am J Physiol Lung Cell Mol Physiol 311: L602–610. [PubMed: 27448665]
24. Lewis BW, Sultana R, Sharma R, Noel A, Langohr I, Patial S, Penn AL, and Saini Y. 2017. Early Postnatal Secondhand Smoke Exposure Disrupts Bacterial Clearance and Abolishes Immune Responses in Muco-Obstructive Lung Disease. J Immunol 199: 1170–1183. [PubMed: 28667160]
25. Goeminne PC, Kicinski M, Vermeulen F, Fierens F, De Boeck K, Nemery B, Nawrot TS, and Dupont LJ. 2013. Impact of air pollution on cystic fibrosis pulmonary exacerbations: a case-crossover analysis. Chest 143: 946–954. [PubMed: 23081770]
26. Kumagai K, Lewandowski RP, Jackson-Humbles DN, Buglak N, Li N, White K, Van Dyken SJ, Wagner JG, and Harkema JR. 2017. Innate Lymphoid Cells Mediate Pulmonary Eosinophilic Inflammation, Airway Mucous Cell Metaplasia, and Type 2 Immunity in Mice Exposed to Ozone. Toxicol Pathol 45: 692–704. [PubMed: 28891433]
27. Peirson SN, and Foster RG. 2011. Bad light stops play. EMBO Rep 12: 380. [PubMed: 21525941]
28. Choudhary I, Vo T, Paudel K, Patial S, and Saini Y. 2021. Compartment-specific transcriptomics of ozone-exposed murine lungs reveals sex- and cell type-associated perturbations relevant to mucoinflammatory lung diseases. Am J Physiol Lung Cell Mol Physiol 320: L99–L125. [PubMed: 33026818]
29. Schindelin J, Arganda-Carreras I, Frise E, Kaynig V, Longair M, Pietzsch T, Preibisch S, Rueden C, Saalfeld S, Schmid B, Tinevez JY, White DJ, Hartenstein V, Eliceiri K, Tomancak P, and Cardona A. 2012. Fiji: an open-source platform for biological-image analysis. Nat Methods 9: 676–682. [PubMed: 22743772]
30. Livraghi A, Grubb BR, Hudson EJ, Wilkinson KJ, Sheehan JK, Mall MA, O'Neal WK, Boucher RC, and Randell SH. 2009. Airway and lung pathology due to mucosal surface dehydration in {beta}-epithelial Na+ channel-overexpressing mice: role of TNF-{alpha} and IL-4R{alpha} signaling, influence of neonatal development, and limited efficacy of glucocorticoid treatment. J Immunol 182: 4357–4367. [PubMed: 19299736]
31. Schneider CA, Rasband WS, and Eliceiri KW. 2012. NIH Image to ImageJ: 25 years of image analysis. Nat Methods 9: 671–675. [PubMed: 22930834]
32. Choudhary I, Vo T, Paudel K, Patial S, and Saini Y. 2020. Compartment-specific transcriptomics of ozone-exposed murine lungs reveals sex and cell type-associated perturbations relevant to mucoinflammatory lung diseases. Am J Physiol Lung Cell Mol Physiol.
33. Lewis BW, Vo T, Choudhary I, Kidder A, Bathula C, Ehre C, Wakamatsu N, Patial S, and Saini Y. 2020. Ablation of IL-33 Suppresses Th2 Responses but Is Accompanied by Sustained Mucus Obstruction in the Scnn1b Transgenic Mouse Model. J Immunol 204: 1650–1660. [PubMed: 32060135]
34. Lewis BW, Choudhary I, Paudel K, Mao Y, Sharma R, Wang Y, Deshane JS, Boucher RC, Patial S, and Saini Y. 2020. The Innate Lymphoid System Is a Critical Player in the Manifestation of Mucoinflammatory Airway Disease in Mice. J Immunol.
35. Michaudel C, Mackowiak C, Maillet I, Fauconnier L, Akdis CA, Sokolowska M, Dreher A, Tan HT, Quesniaux VF, Ryffel B, and Togbe D. 2018. Ozone exposure induces respiratory barrier biphasic injury and inflammation controlled by IL-33. J Allergy Clin Immunol 142: 942–958. [PubMed: 29331644]
36. Sokolowska M, Quesniaux VFJ, Akdis CA, Chung KF, Ryffel B, and Togbe D. 2019. Acute Respiratory Barrier Disruption by Ozone Exposure in Mice. Front Immunol 10: 2169. [PubMed: 31608051]
37. Joyner BL, Jones SW, Cairns BA, Harris BD, Coverstone AM, Abode KA, Ortiz-Pujols SM, Kocis KC, and Noah TL. 2013. DNA and inflammatory mediators in bronchoalveolar lavage fluid from children with acute inhalational injuries. J Burn Care Res 34: 326–333. [PubMed: 23128126]

38. Kirchner KK, Wagener JS, Khan TZ, Copenhaver SC, and Accurso FJ. 1996. Increased DNA levels in bronchoalveolar lavage fluid obtained from infants with cystic fibrosis. Am J Respir Crit Care Med 154: 1426–1429. [PubMed: 8912759]
39. Hendrix AY, and Kheradmand F. 2017. The Role of Matrix Metalloproteinases in Development, Repair, and Destruction of the Lungs. Prog Mol Biol Transl Sci 148: 1–29. [PubMed: 28662821]
40. Finlay GA, O'Driscoll LR, Russell KJ, D'Arcy EM, Masterson JB, FitzGerald MX, and O'Connor CM. 1997. Matrix metalloproteinase expression and production by alveolar macrophages in emphysema. Am J Respir Crit Care Med 156: 240–247. [PubMed: 9230755]
41. Trojanek JB, Cobos-Correa A, Diemer S, Kormann M, Schubert SC, Zhou-Suckow Z, Agrawal R, Duerr J, Wagner CJ, Schatterny J, Hirtz S, Sommerburg O, Hartl D, Schultz C, and Mall MA. 2014. Airway mucus obstruction triggers macrophage activation and matrix metalloproteinase 12-dependent emphysema. Am J Respir Cell Mol Biol 51: 709–720. [PubMed: 24828142]
42. Kumagai K, Lewandowski R, Jackson-Humbles DN, Li N, Van Dyken SJ, Wagner JG, and Harkema JR. 2016. Ozone-Induced Nasal Type 2 Immunity in Mice Is Dependent on Innate Lymphoid Cells. Am J Respir Cell Mol Biol 54: 782–791. [PubMed: 26559808]
43. Lewis BW, Choudhary I, Paudel K, Mao Y, Sharma R, Wang Y, Deshane JS, Boucher RC, Patial S, and Saini Y. 2020. The Innate Lymphoid System Is a Critical Player in the Manifestation of Mucoinflammatory Airway Disease in Mice. J Immunol 205: 1695–1708. [PubMed: 32817334]
44. Sitkauskiene B, Johansson AK, Sergejeva S, Lundin S, Sjostrand M, and Lotvall J. 2004. Regulation of bone marrow and airway CD34+ eosinophils by interleukin-5. Am J Respir Cell Mol Biol 30: 367–378. [PubMed: 12920051]
45. Menzies-Gow A, Ying S, Phipps S, and Kay AB. 2004. Interactions between eotaxin, histamine and mast cells in early microvascular events associated with eosinophil recruitment to the site of allergic skin reactions in humans. Clin Exp Allergy 34: 1276–1282. [PubMed: 15298570]
46. Rosenberg HF, Phipps S, and Foster PS. 2007. Eosinophil trafficking in allergy and asthma. J Allergy Clin Immunol 119: 1303–1310; quiz 1311-1302. [PubMed: 17481712]
47. Becker S, Quay J, and Koren HS. 1991. Effect of ozone on immunoglobulin production by human B cells in vitro. J Toxicol Environ Health 34: 353–366. [PubMed: 1834858]
48. Elborn JS 2016. Cystic fibrosis. Lancet 388: 2519–2531. [PubMed: 27140670]
49. Khan TZ, Wagener JS, Bost T, Martinez J, Accurso FJ, and Riches DW. 1995. Early pulmonary inflammation in infants with cystic fibrosis. Am J Respir Crit Care Med 151: 1075–1082. [PubMed: 7697234]
50. Armstrong DS, Grimwood K, Carlin JB, Carzino R, Gutierrez JP, Hull J, Olinsky A, Phelan EM, Robertson CF, and Phelan PD. 1997. Lower airway inflammation in infants and young children with cystic fibrosis. Am J Respir Crit Care Med 156: 1197–1204. [PubMed: 9351622]
51. Armstrong DS, Grimwood K, Carzino R, Carlin JB, Olinsky A, and Phelan PD. 1995. Lower respiratory infection and inflammation in infants with newly diagnosed cystic fibrosis. BMJ 310: 1571–1572. [PubMed: 7787647]
52. Mott LS, Park J, Murray CP, Gangell CL, de Klerk NH, Robinson PJ, Robertson CF, Ranganathan SC, Sly PD, Stick SM, and Arest CF. 2012. Progression of early structural lung disease in young children with cystic fibrosis assessed using CT. Thorax 67: 509–516. [PubMed: 22201161]
53. Mott LS, Park J, Gangell CL, de Klerk NH, Sly PD, Murray CP, Stick SM, and G. Australian Respiratory Early Surveillance Team for Cystic Fibrosis Study. 2013. Distribution of early structural lung changes due to cystic fibrosis detected with chest computed tomography. J Pediatr 163: 243–248 e241-243. [PubMed: 23357185]
54. Herring MJ, Putney LF, Wyatt G, Finkbeiner WE, and Hyde DM. 2014. Growth of alveoli during postnatal development in humans based on stereological estimation. Am J Physiol Lung Cell Mol Physiol 307: L338–344. [PubMed: 24907055]
55. Dutta S, and Sengupta P. 2016. Men and mice: Relating their ages. Life Sci 152: 244–248. [PubMed: 26596563]
56. Gehrig S, Duerr J, Weitnauer M, Wagner CJ, Graeber SY, Schatterny J, Hirtz S, Belaaouaj A, Dalpke AH, Schultz C, and Mall MA. 2014. Lack of neutrophil elastase reduces inflammation, mucus hypersecretion, and emphysema, but not mucus obstruction, in mice with cystic fibrosis-like lung disease. Am J Respir Crit Care Med 189: 1082–1092. [PubMed: 24678594]

57. Livraghi-Butrico A, Grubb BR, Wilkinson KJ, Volmer AS, Burns KA, Evans CM, O'Neal WK, and Boucher RC. 2017. Contribution of mucus concentration and secreted mucins Muc5ac and Muc5b to the pathogenesis of muco-obstructive lung disease. Mucosal Immunol 10: 395–407. [PubMed: 27435107]

Key Points:

1. Ozone induces alveolar space remodeling in the developing lungs.
2. Ozone promotes Type 2 mucoinflammation in the developing lungs.
3. Ozone worsens mucoinflammatory responses in ongoing CF-like lung disease.

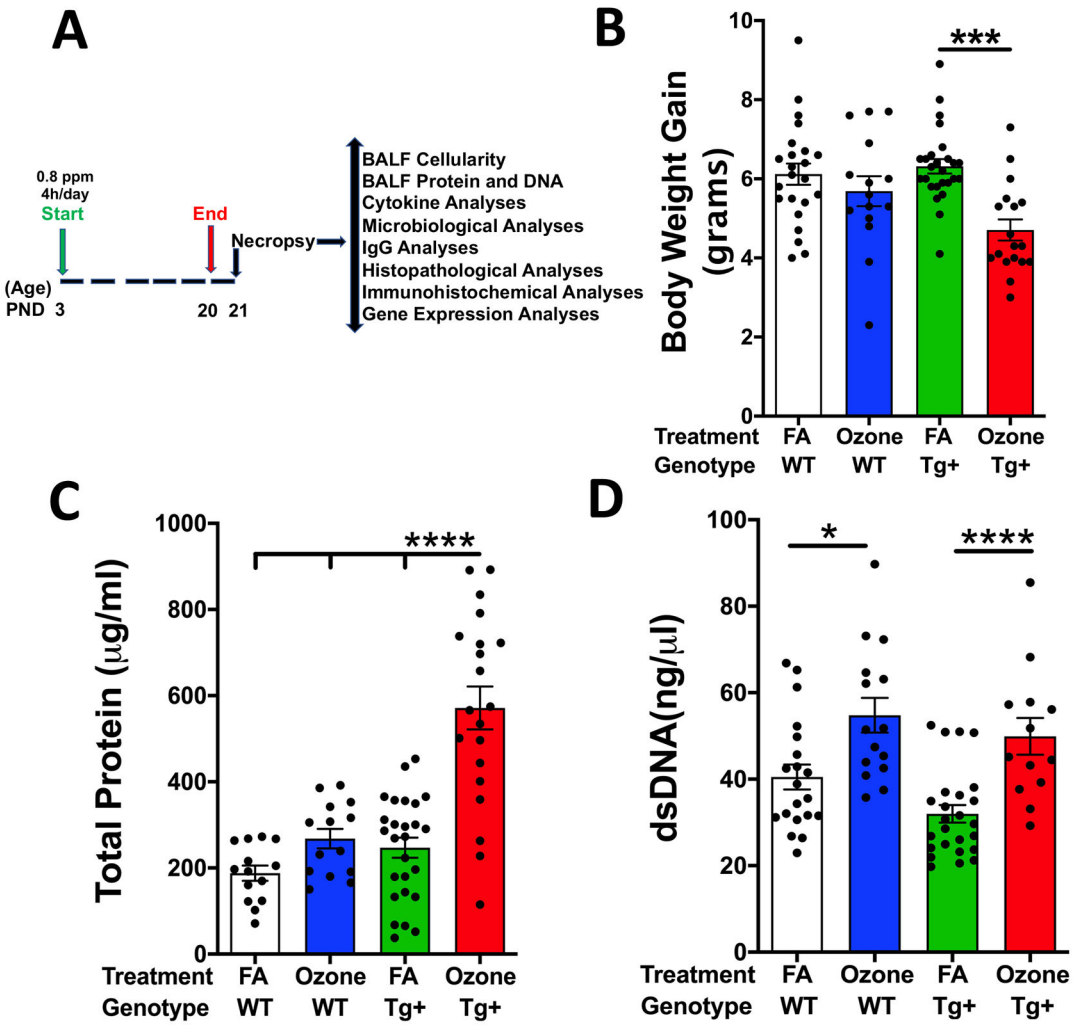

Fig. 1: Ozone exposure disrupts body weight gain and compromises epithelial-endothelial barrier in *Scnn1b*-Tg+ neonates.

(A) Experimental design depicting exposure regimen and designated outcomes examined. **(B)** Bodyweight gain over the 18 days of exposure (PND 3-20) to filtered air (FA) or ozone in WT and *Scnn1b*-Tg+ mice **(C)** Total protein concentration (µg/ml) in the cell-free bronchoalveolar lavage fluid (BALF) from FA- and ozone- exposed WT and *Scnn1b*-Tg+ mice **(D)** Double-stranded DNA (dsDNA) concentration (ng/µl) in the cell-free BALF from FA- and ozone-exposed WT and *Scnn1b*-Tg+ mice. Error bars represent SEM. *p<0.05, ***p<0.001, ****p<0.0001 using one-way ANOVA followed by Tukey's multiple comparison post hoc test.

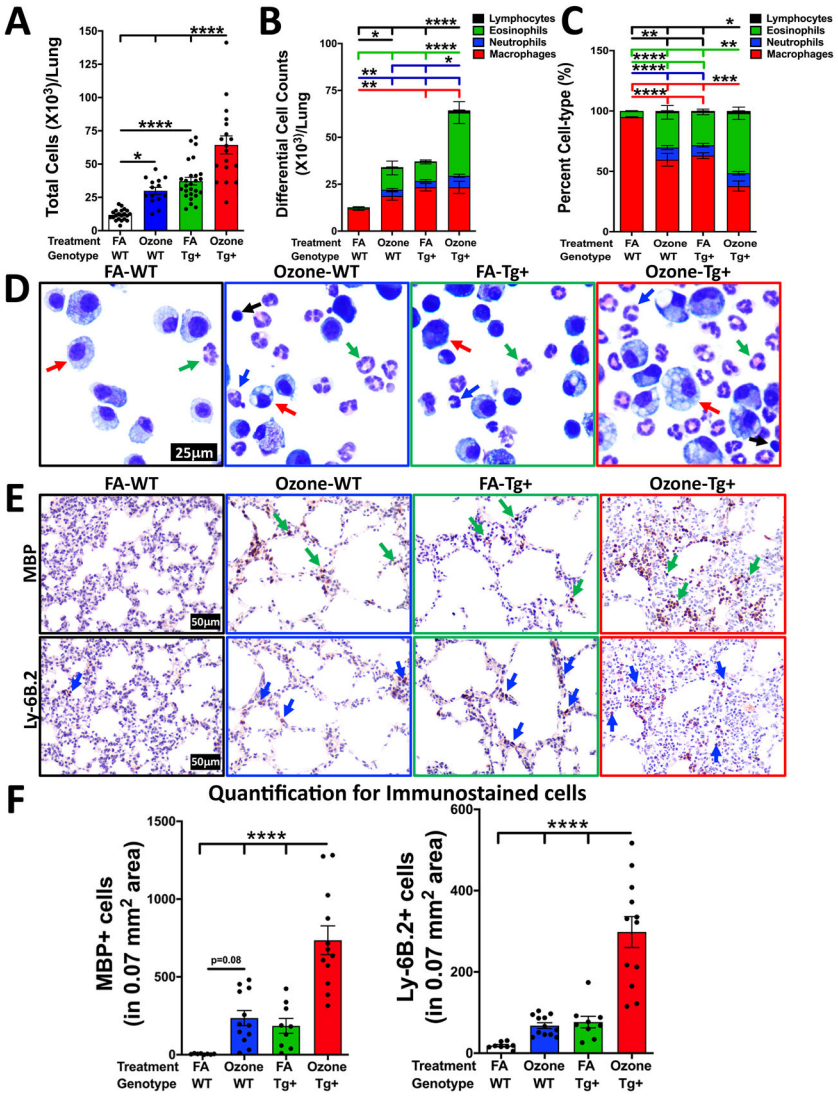

Fig. 2: Ozone exposure alters immune cell composition in the lung airspaces of WT and *Scnn1b*-Tg+ mice

(A) Total cells recovered per right lung in the harvested BALF from 21-d-old FA- and ozone- exposed WT and *Scnn1b*-Tg+mice. (**B**) Differential cell counts and **(C)** their respective percentages are shown as a stacked bar graph [BALF macrophages (red), neutrophils (blue), eosinophils (green), lymphocytes (black)]. Error bars represent SEM. *p<0.05, **p<0.01, ***p<0.001, ****p<0.0001 using one-way ANOVA followed by Tukey's multiple comparison post hoc test. **(D)** Representative photomicrographs of Wright-Giemsa stained BALF cytospins from FA-exposed WT (FA-WT), Ozone-exposed WT (ozone-WT), FA-exposed *Scnn1b*-Tg+ mice (FA-Tg+), ozone-exposed *Scnn1b*-Tg+ (ozone-Tg+) at PND 21. Macrophages (red arrows), neutrophils (blue arrows), eosinophils (green arrows), and lymphocytes (black arrows). All photomicrographs in panel D were taken at the same magnification. **(E)** Representative photomicrographs of Major Basic Protein (MBP) (upper panels) and Ly6B.2 (bottom panels) stained lung sections from FA-WT, ozone-WT, FA-Tg+, and ozone-Tg+ mice. All photomicrographs in panel E were taken

at the same magnification. **(F)** Image J quantification of Major Basic Protein (MBP) (left panel) and Ly6B.2 (right panels) stained cells per unit area analyzed. Error bars represent SEM. ****$p<0.0001$ using one-way ANOVA followed by Tukey's multiple comparison post hoc test.

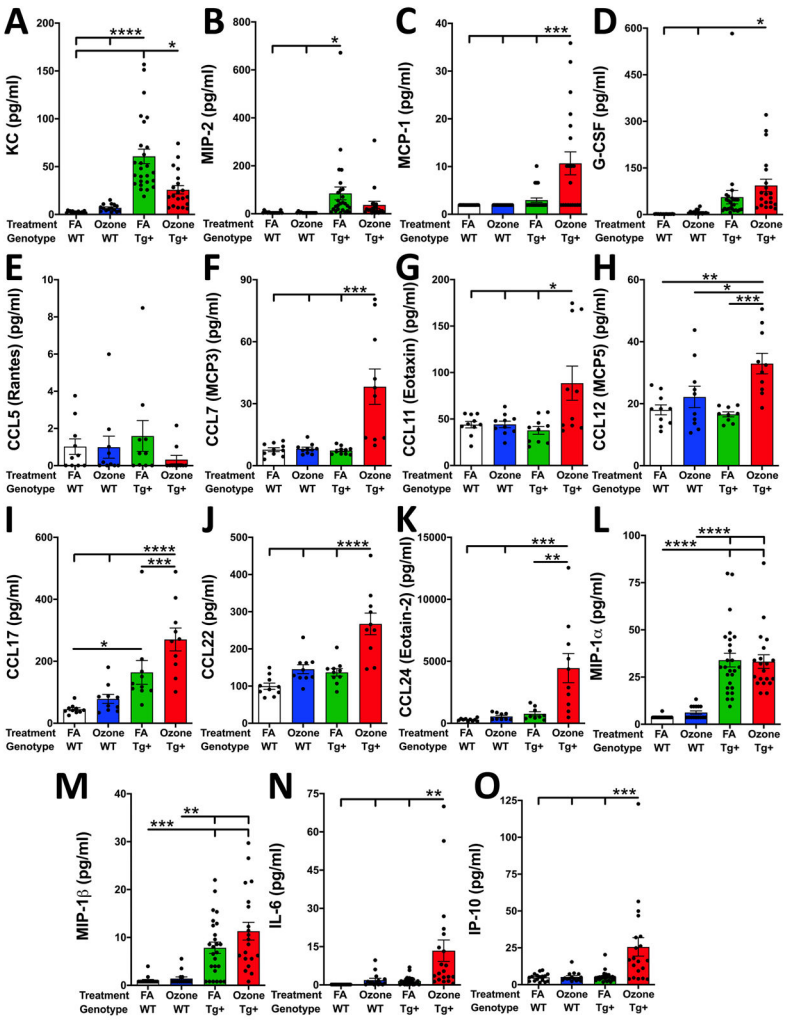

Fig. 3: Ozone exposure alters the cytokine levels in WT and *Scnn1b*-Tg+ mice.

Cytokine levels (pg/ml; picograms per milliliter) of **(A)** KC, **(B)** MIP-2, **(C)** MCP-1, and **(D)** G-CSF in BALF from FA-WT (white bar), ozone-WT (blue bar), FA-Tg+ (green bar), ozone-Tg+ (red Bar) mice. Cytokine levels (pg/ml; picograms per milliliter; total protein contents- 2.34mg/ml) of **(E)** CCL5, **(F)** CCL7**, (G)** CCL11, **(H)** CCL12, **(I)** CCL17, **(J)** CCL22, and **(K)** CCL24 in lung homogenate from FA-WT (white bar), ozone-WT (blue bar), FA-Tg+ (green bar), ozone-Tg+ (red Bar) mice. Cytokine levels (pg/ml; picograms per milliliter) of **(L)** MIP-1α, **(M)** MIP-1β, **(N)** IL-6, **(O)** IP-10 in BALF from FA-WT (white bar), ozone-WT (blue bar), FA-Tg+ (green bar), ozone-Tg+ (red Bar) mice. Error bars represent SEM. *p<0.05, **p<0.01 ***p<0.001, ****p<0.0001 using one-way ANOVA followed by Tukey's multiple comparison post hoc test.

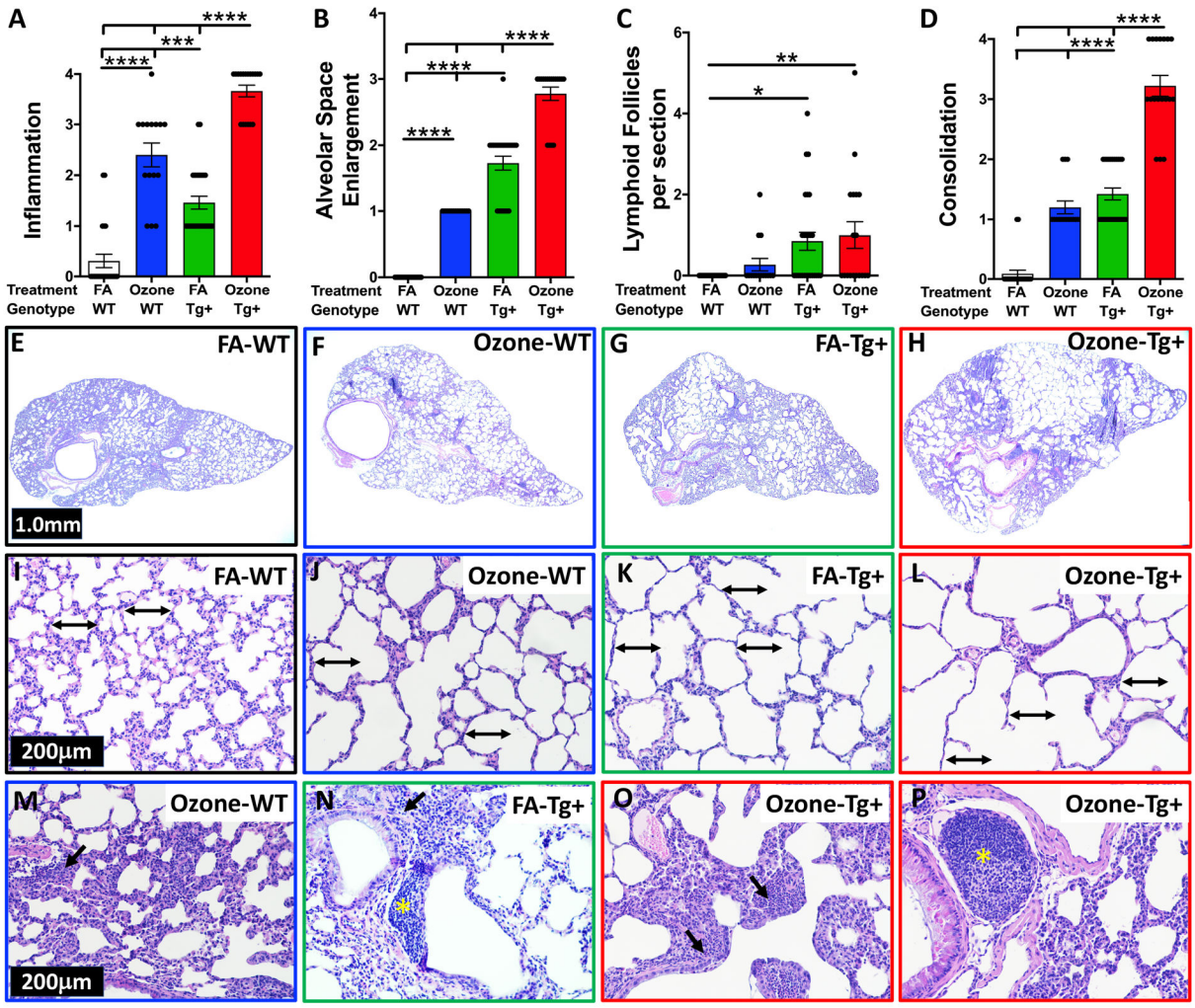

Fig. 4: Ozone exposure exacerbates lung pathology in WT and *Scnn1b*-Tg+ mice.

Semiquantitative histopathological scores for **(A)** peribronchiolar and perivascular inflammation, **(B)** alveolar space enlargement, **(C)** lymphoid follicles per section, and **(D)** alveolar space thickening/consolidation in FA-WT (white bar), ozone-WT (blue bar), FA-Tg+ (green bar) and ozone-Tg+ (red bar) mice. Error bars represent SEM. *p<0.05, **p<0.01 ***p<0.001, ****p<0.0001 using one-way ANOVA followed by Tukey's multiple comparison post hoc test. Representative photomicrographs from H & E stained, left lung lobe sections from 21-day-old FA-WT **(E, I)**, ozone-WT **(F, J, M)**, FA-Tg+ **(G, K, N)**, and ozone-Tg+ **(H, L, O, P)** mice. Double-headed arrows (all with similar dimensions) depict linear alveolar airspace width **(I, J, K, L)**; Black arrows (**M, N, O**) depict immune cell infiltration in peribronchiolar spaces. Yellow asterisks (**P**) depict lymphoid aggregates (BALTs). All photomicrographs were taken at the same magnification.

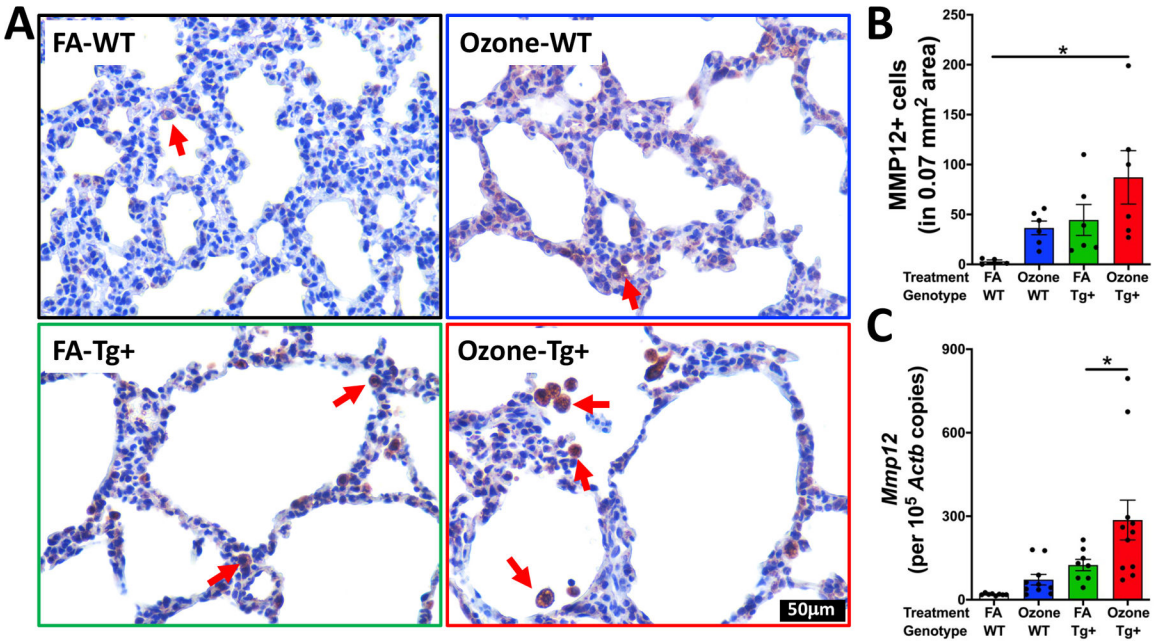

Fig. 5: Ozone exposure increases expression of MMP12 in *Scnn1b*-Tg+ mice.

(A) Representative images from sections stained for immunolocalization of MMP-12 protein in FA-WT, ozone-WT, FA-Tg+, and ozone-Tg+ lungs. **(B)** Image J quantification of MMP12 stained cells per unit area analyzed. Error bars represent SEM. *p<0.05 using one-way ANOVA followed by Tukey's multiple comparison post hoc test. **(C)** Absolute quantification of *Mmp12* mRNA expression in whole lung lysate from FA-WT (white bar), ozone-WT (blue bar), FA-Tg+ (green bar), and ozone-Tg+ (red bar) mice. Error bars represent SEM. *p<0.05, using one-way ANOVA followed by Tukey's multiple comparison post hoc test. Red arrows depict macrophages positively stained for MMP12. All photomicrographs were taken at the same magnification.

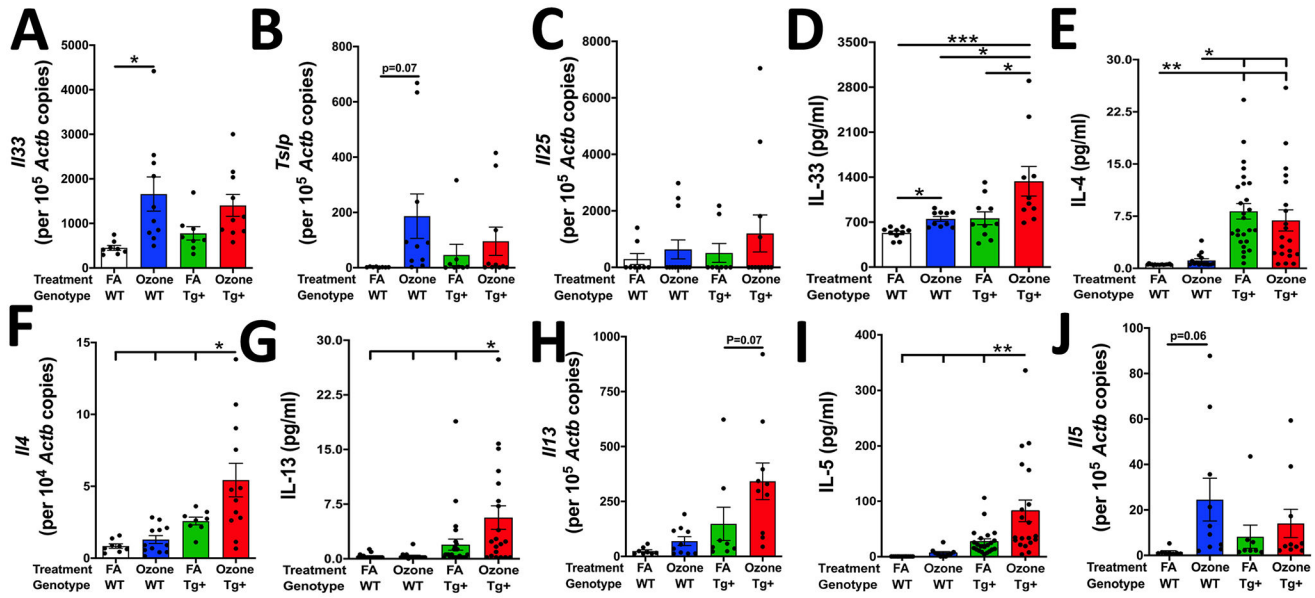

Fig. 6: Ozone exposure induces type 2 inflammation in the airspaces.

Absolute quantification of **(A)** *Il33* mRNA, **(B)** *Tslp* mRNA, **(C)** *Il25* mRNA in lungs from FA-WT (white bar), ozone-WT (blue bar), FA-Tg+ (green bar), and ozone-Tg+ (red bar) mice. **(D)** IL-33 cytokine levels (pg/ml; picograms per milliliter; total protein contents-2.34mg/ml) in lung homogenate. **(E)** BALF cytokine levels (pg/ml; picograms per milliliter) of IL-4. **(F)** Absolute quantification of *Il4* mRNA. **(G)** BALF cytokine levels (pg/ml; picograms per milliliter) of IL-13. **(H)** Absolute quantification of *Il13* mRNA. **(I)** BALF cytokine levels (pg/ml; picograms per milliliter) of IL-5. **(J)** Absolute quantification of *Il5* mRNA in FA-WT (white bar), ozone-WT (blue bar), FA-Tg+ (green bar), and ozone-Tg+ (red bar) mice. Error bars represent SEM. *p<0.05, **p<0.01, ***p<0.001 using one-way ANOVA followed by Tukey's multiple comparison post hoc test.

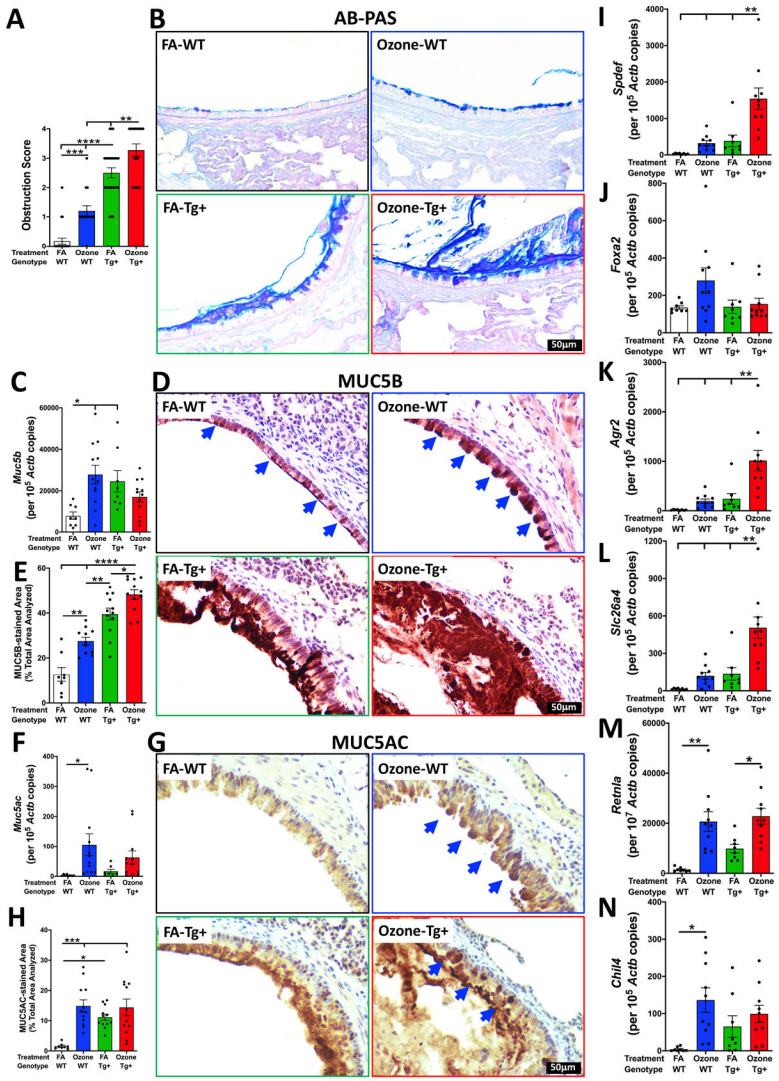

Fig. 7: Ozone promotes mucus obstruction, mucous cell metaplasia, and expression of mucoinflammatory genes associated with mucous cell metaplasia, mucus production, and type 2 inflammation in WT and *Scnn1b*-Tg+ mice.

(A) Quantification of airway mucus obstruction from AB-PAS stained left lung lobe histological sections from FA-WT (white bar), ozone-WT (blue bar), FA-Tg+ (green bar), and ozone-Tg+ (red bar) mice. **(B)** Representative micrographs of AB-PAS stained lung sections from FA-WT, ozone-WT, FA-Tg+, and ozone-Tg+ groups. All photomicrographs were taken at the same magnification. **(C)** Absolute quantification of *Muc5b* mRNA and **(D)** Representative photomicrographs of MUC5B stained left lung lobe histological sections from FA-WT, ozone-WT, FA-Tg+, and ozone-Tg+ groups. All photomicrographs were taken at the same magnification. **(E)** Percent MUC5B stained area in the first-generation airway section using ImageJ software. **(F)** Absolute quantification of *Muc5ac* mRNA and **(G)** Representative photomicrographs of MUC5AC stained left lung lobe histological sections from FA-WT, ozone-WT, FA-Tg+, and ozone-Tg+ groups. **(H)** Percent MUC5AC stained area in the first-generation airway section using ImageJ software. All photomicrographs were taken at the same magnification. Error bars represent SEM.

*p<0.05, **p<0.01, ***p<0.001, ****p<0.0001 using one-way ANOVA followed by Tukey's multiple comparison post hoc test. Absolute quantification of *Spdef* mRNA **(I)**, *Foxa2* mRNA **(J)**, *Agr2* mRNA **(K)**, *Slc26a4* mRNA **(L)**, *Retnla* mRNA **(M)**, and *Chil4* mRNA **(N)** in FA-WT (white bar), ozone-WT (blue bar), FA-Tg+ (green bar), and ozone-Tg+ (red bar) mice. Error bars represent SEM. *p<0.05, **p<0.01 using one-way ANOVA followed by Tukey's multiple comparison post hoc test.

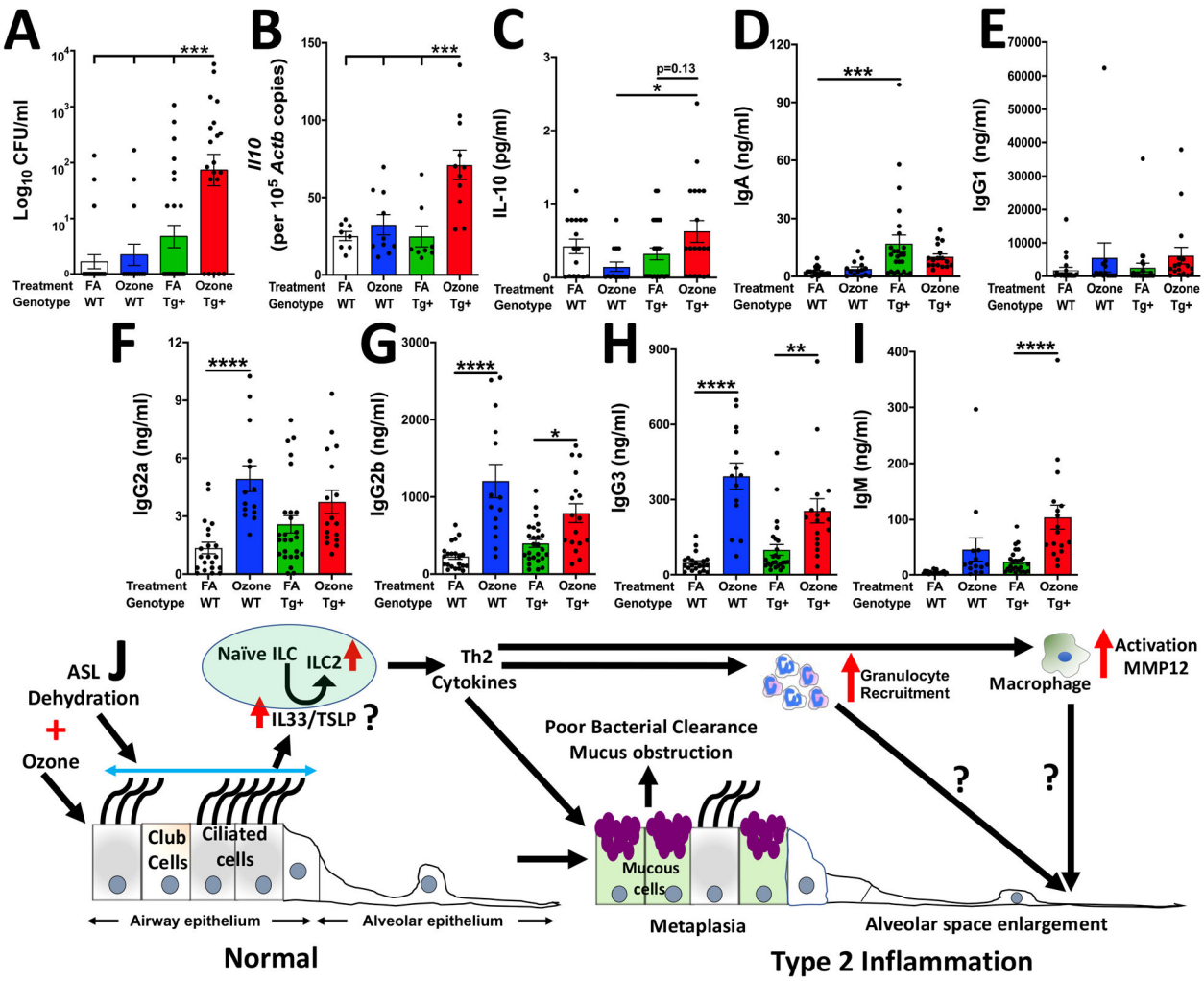

Fig. 8: Ozone disrupts bacterial clearance in *Scnn1b*-Tg+ *mice.*

(A) Colony Forming Units (CFU) in BALF from FA-WT (white bar), ozone-WT (blue bar), FA-Tg+ (green bar), and ozone-Tg+ (red bar) mice. The CFU values were $\log_{10}$-transformed with an offset of +1 ($\log_{10}$ +1 transformation). **(B)** Absolute quantification of *Il10* mRNA and **(C)** BALF cytokine levels (pg/ml; picograms per milliliter) of IL-10 in FA-WT (white bar), ozone-WT (blue bar), FA-Tg+ (green bar), and ozone-Tg+ (red bar) mice. BALF immunoglobulin levels of IgA **(D)**, IgG1 **(E)**, IgG2a **(F),** IgG2b **(G)**, IgG3 **(H)**, and IgM **(I)** in cell-free BALF from FA-WT (white bar), ozone-WT (blue bar), FA-Tg+ (green bar), and ozone-Tg+ (red bar) mice. Error bars represent SEM. *p<0.05, **p<0.01, ***p<0.001, ****p<0.0001 using one-way ANOVA followed by Tukey's multiple comparison post hoc test. **(J)** Hypothetical model for the interaction of ozone and airway surface liquid dehydration in the manifestation of Type 2 mucoinflammatory disease. Vertical Red arrows indicate increased responses to ozone/airway surface liquid dehydration. Arrows with associated question marks (?) suggest a need for further investigation.